Electronic Supplementary Information for:

N-Heterocyclic Carbene and Cyclic (Alkyl)(amino)carbene Complexes of Vanadium(III) and Vanadium(V)

Günther Horrer[a], Ivo Krummenacher[a,b], Sophie Mann[a], Holger Braunschweig[a,b] and Udo Radius[a]*.

[a]Institut für Anorganische Chemie, Julius-Maximilians-Universität Würzburg, Am Hubland, 97074 Würzburg, Germany.

[b]Institute for Sustainable Chemistry & Catalysis with Boron, Julius-Maximilians-Universität Würzburg, Am Hubland, 97074 Würzburg, Germany.

Table of Contents:

1) NMR spectra of the compounds

NMR spectra of [(IDipp)$VOCl_3$] 12

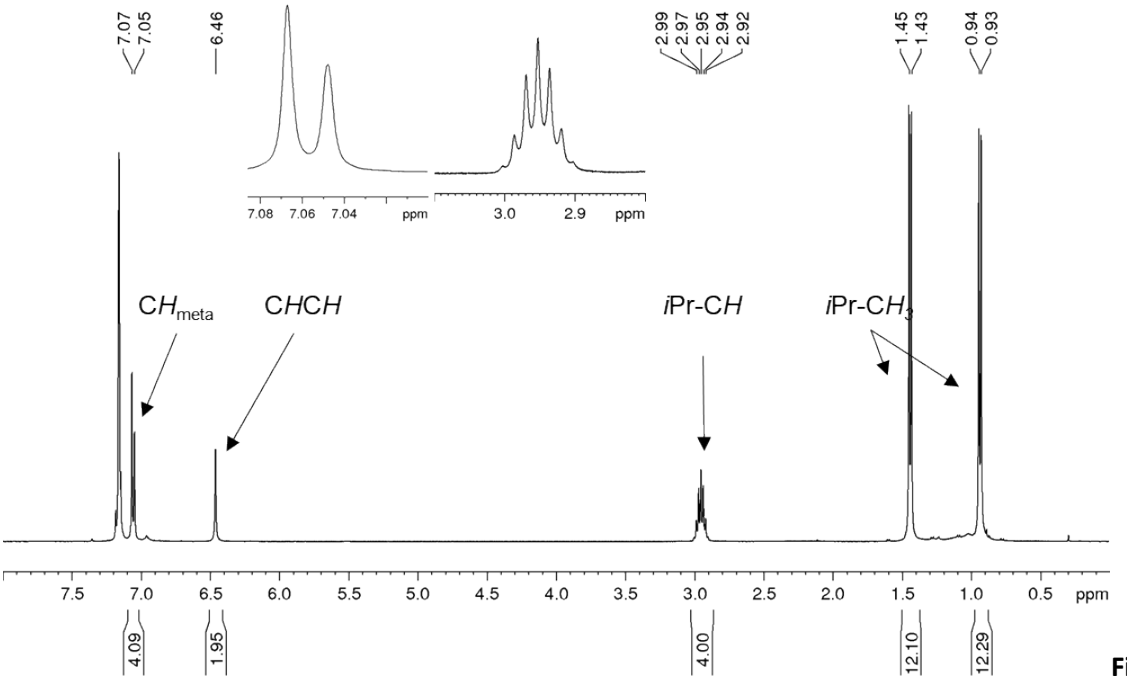

Figure S1: ^{1}H-NMR-spectrum of [(IDipp)$VOCl_3$] **12** in C_6D_6. The signal for the *para*-positioned protons is hidden by the residual proton resonance of C_6D_5H (the signals were assigned *via* HSQC and HMBC correlation experiments).

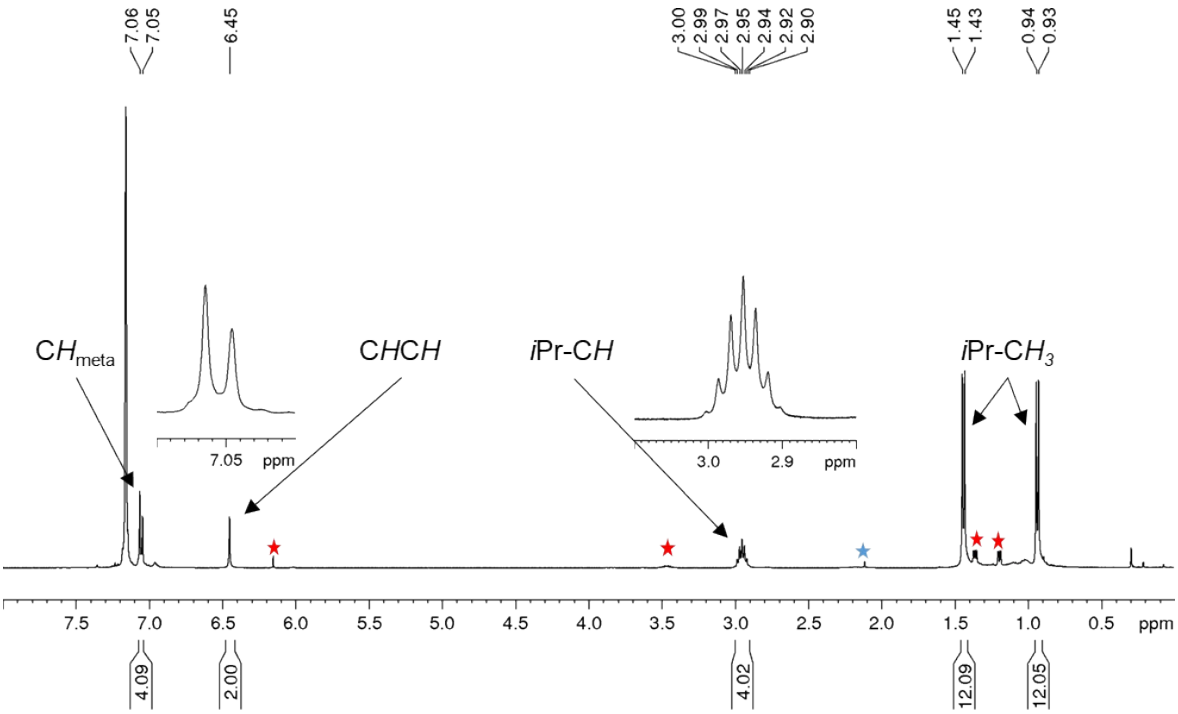

Figure S2: ^{1}H-NMR-spectrum of [(IDipp)$VOCl_3$] **12** in C_6D_6. The signal for the *para*-positioned protons is hidden by the residual proton resonance of C_6D_5H (the signals were assigned *via* HSQC and HMBC correlation experiments). Red asterisk: residual decomposition signals of a IPr species. Blue asterisk: residual toluene signal.

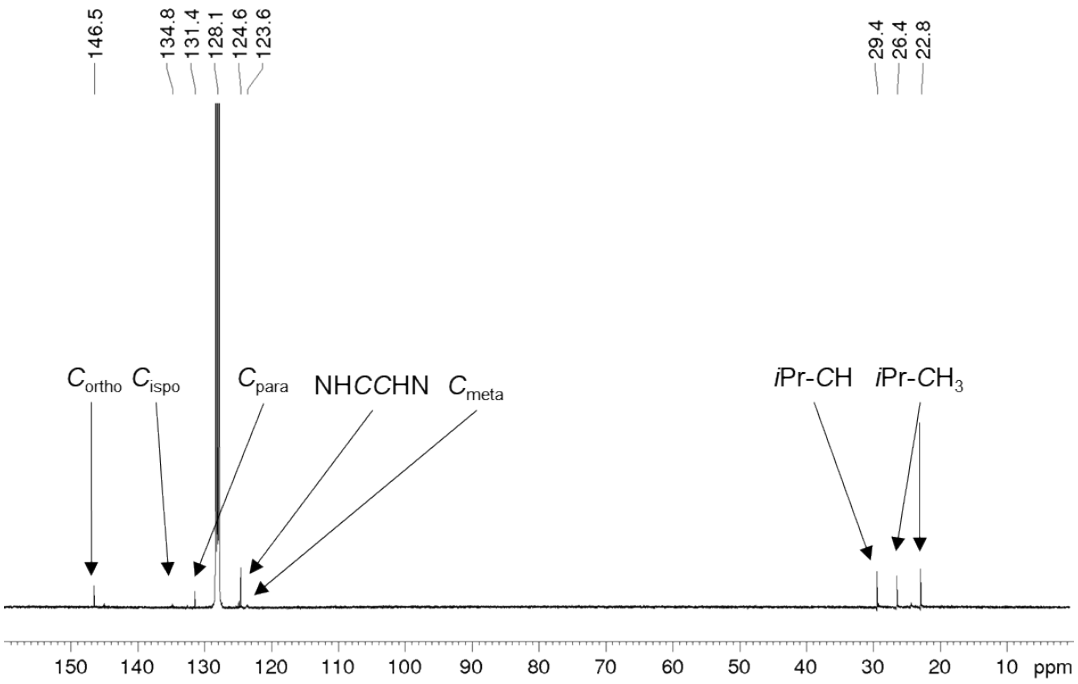

Figure S3: ^{13}C-NMR spectrum of [(IDipp)VOCl$_3$] **12** in C_6D_6. The carbene carbon atom was not detected due to the quadrupole moment of ^{51}V.

NMR spectra of [(SIDippVOCl$_3$] 13

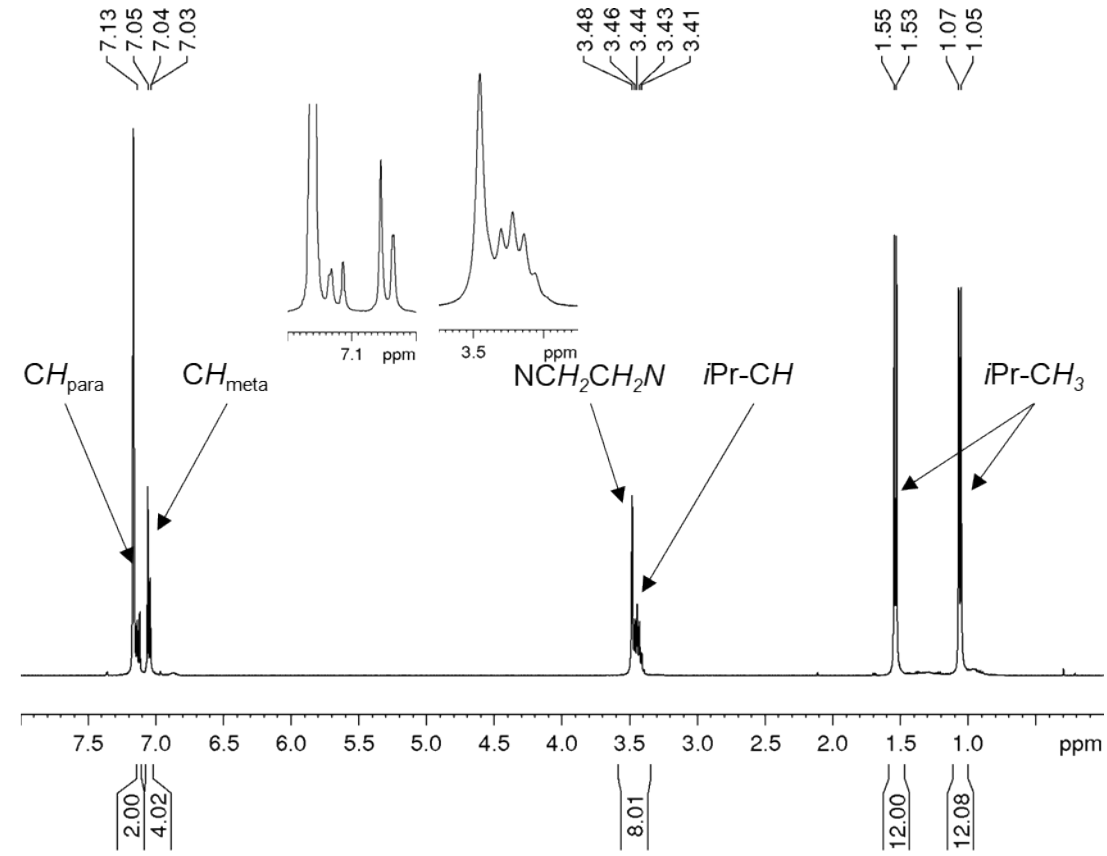

Figure S4: ^{1}H-NMR-spectrum of [(SIDipp)VOCl$_3$] **13** C_6D_6.

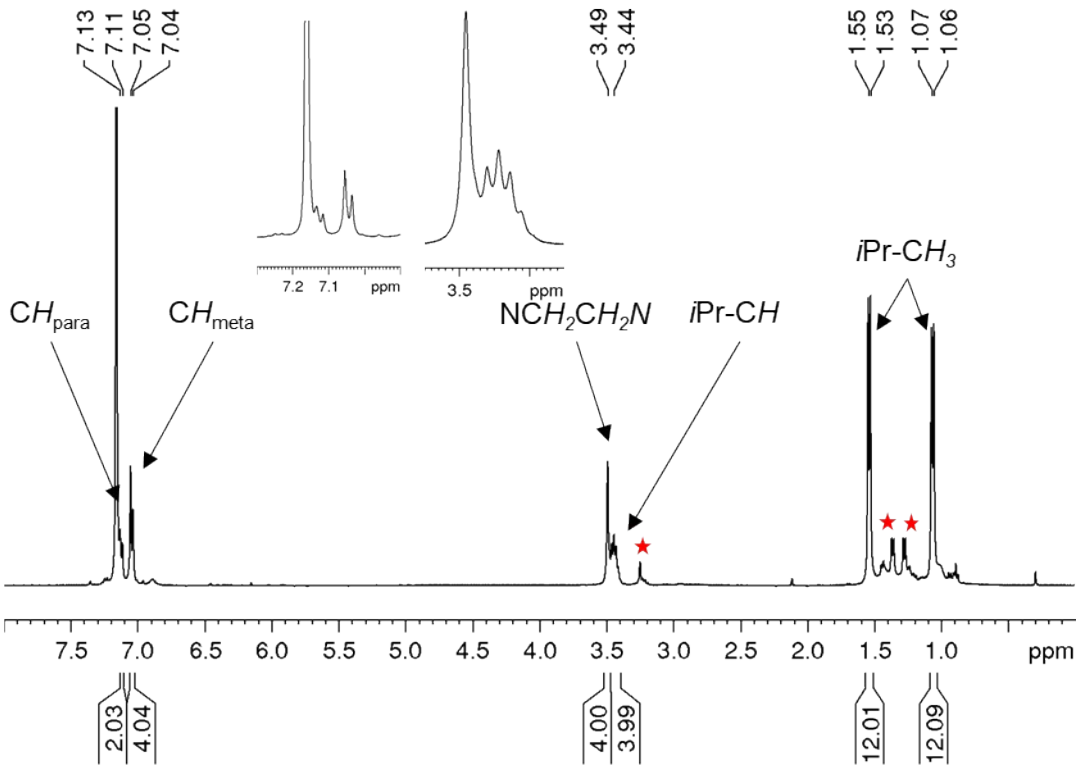

Figure S5: ^{1}H-NMR-spectrum of the reaction of [(SIDipp)VCl_3] **5** C_6D_6 with oxygen. Red asterisk: residual decomposition signals of a SIPr species.

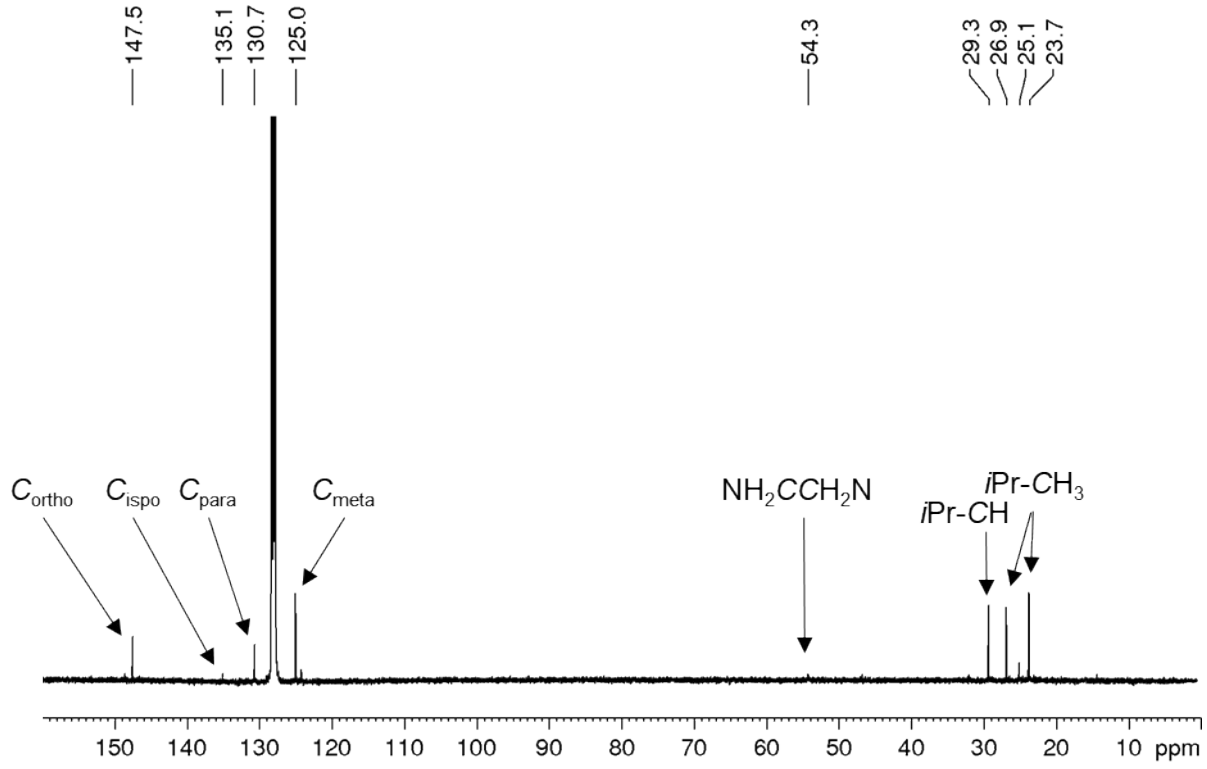

Figure S6: ^{13}C-NMR spectrum of [(SIDipp)$VOCl_3$] **13** in C_6D_6. The carbene carbon atom was not detected.

NMR Spectra of [V(N-*p*-$CH_3C_6H_4$)Cl_3(IDipp)] 14

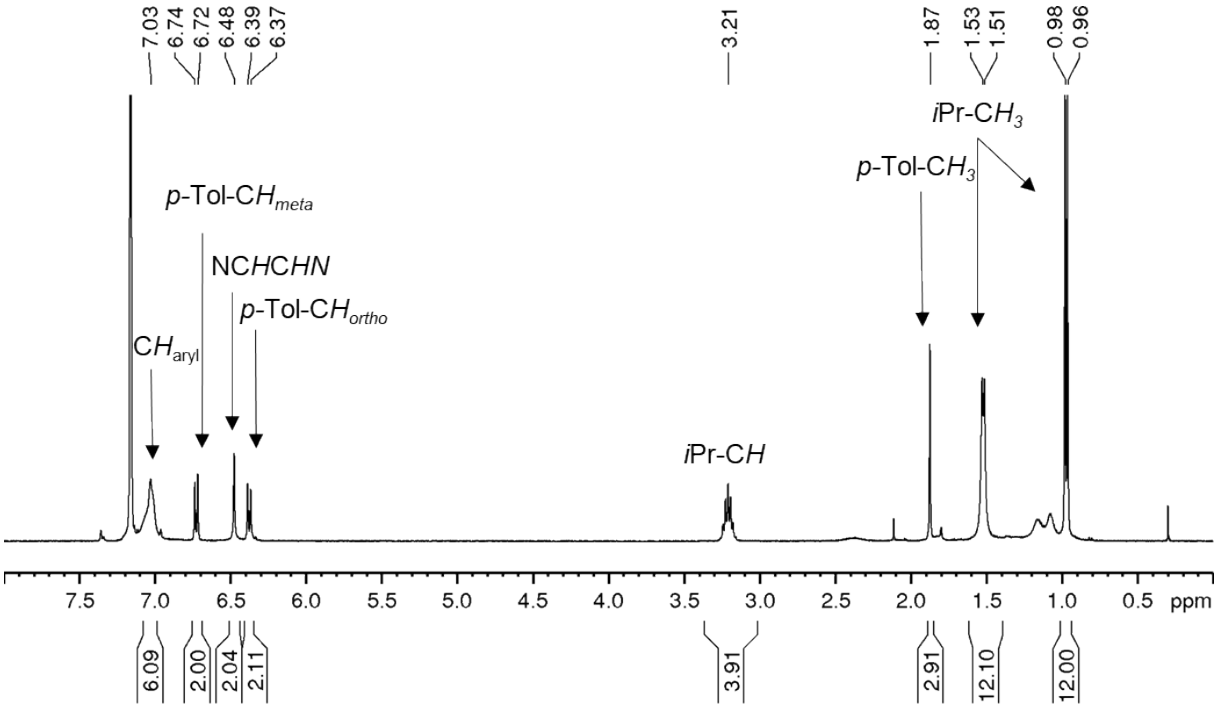

Figure S7: ^{1}H-NMR spectrum of [V(N-*p*-$CH_3C_6H_4$)Cl_3(IDipp)] **14** in C_6D_6.

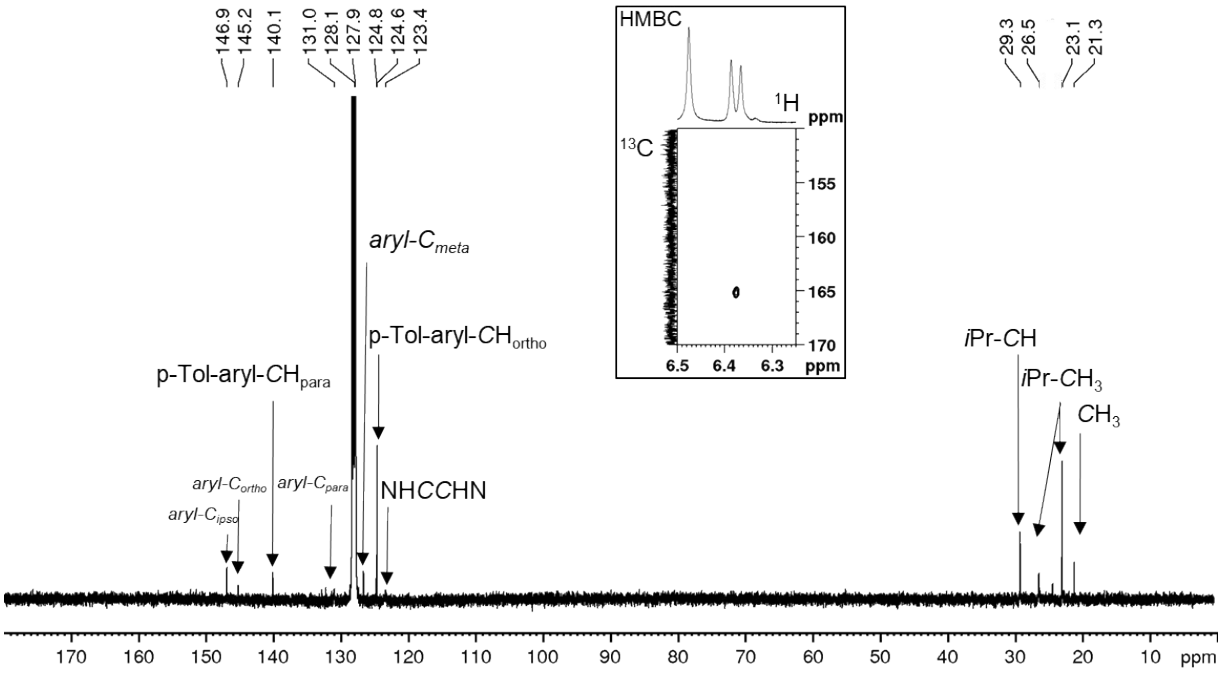

Figure S8: $^{13}C\{^1H\}$-NMR spectrum of [V(N-*p*-$CH_3C_6H_4$)Cl_3(IDipp)] **14** in C_6D_6. The carbon resonances for *p*-Tol-aryl-*C*H*meta* at 127.7 ppm coincides with the solvent resonances. The *p*-Tol-*aryl*-C_{ipso} resonances at 165.1 ppm were resolved with HMBC experiments. The carbene carbon atom was not detected.

NMR Spectra of [V(N-*p*-FC_6H_4)Cl_3(IDipp)] 15

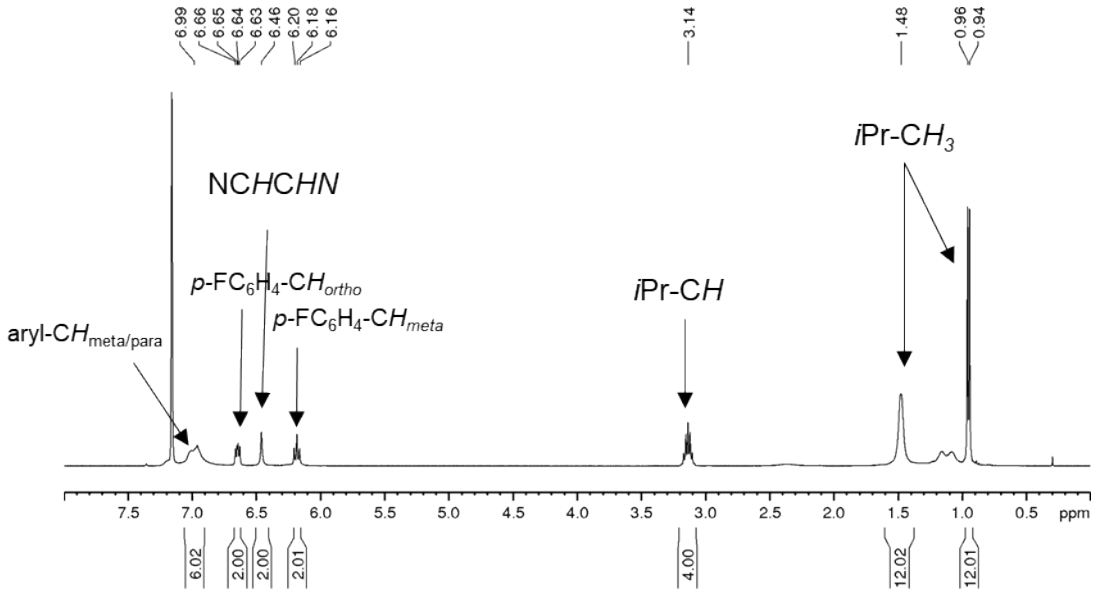

Figure S9: ^{1}H NMR spectrum of [V(N-*p*-FC_6H_4)Cl_3(IDipp)] **15** in C_6D_6.

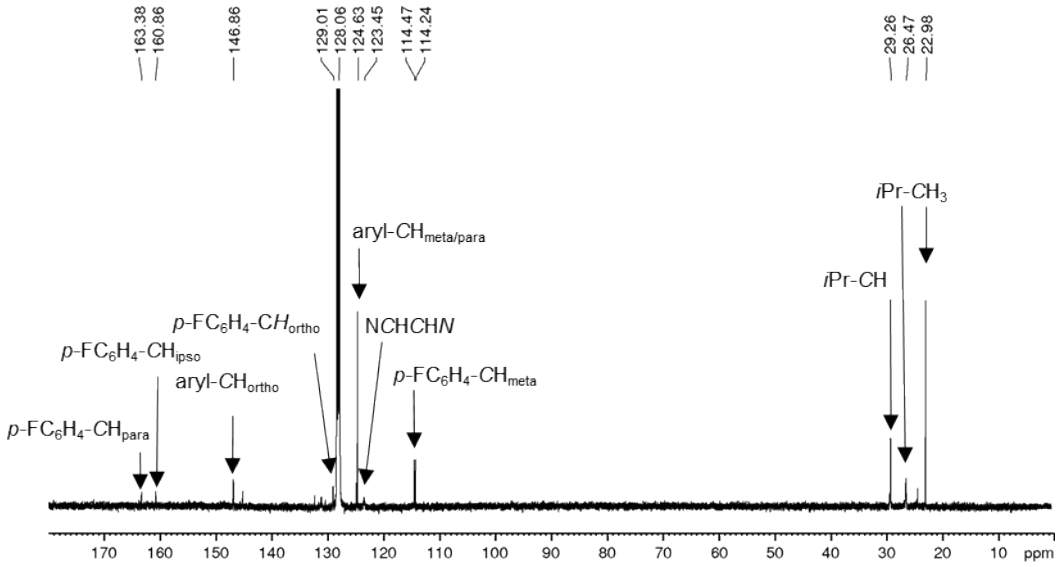

Figure S10: $^{13}C\{^{1}H\}$ NMR spectrum of [V(N-*p*-FC_6H_4)Cl_3(IDipp)] **15** in C_6D_6. The resonance for the carbene carbon atom was not detected.

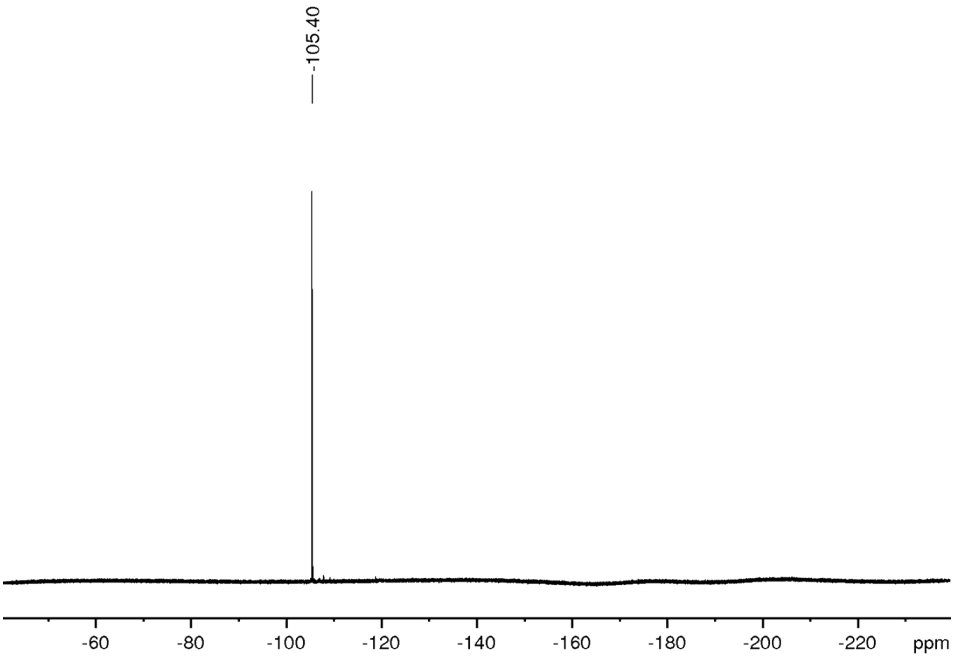

Figure S11: $^{19}F\{^{1}H\}$ NMR spectrum of [V(N-*p*-FC_6H_4)Cl_3(IDipp)] **15** in C_6D_6.

NMR Spectra of [V(N-*p*-$CH_3C_6H_4$)Cl_3(SIDipp)] 16

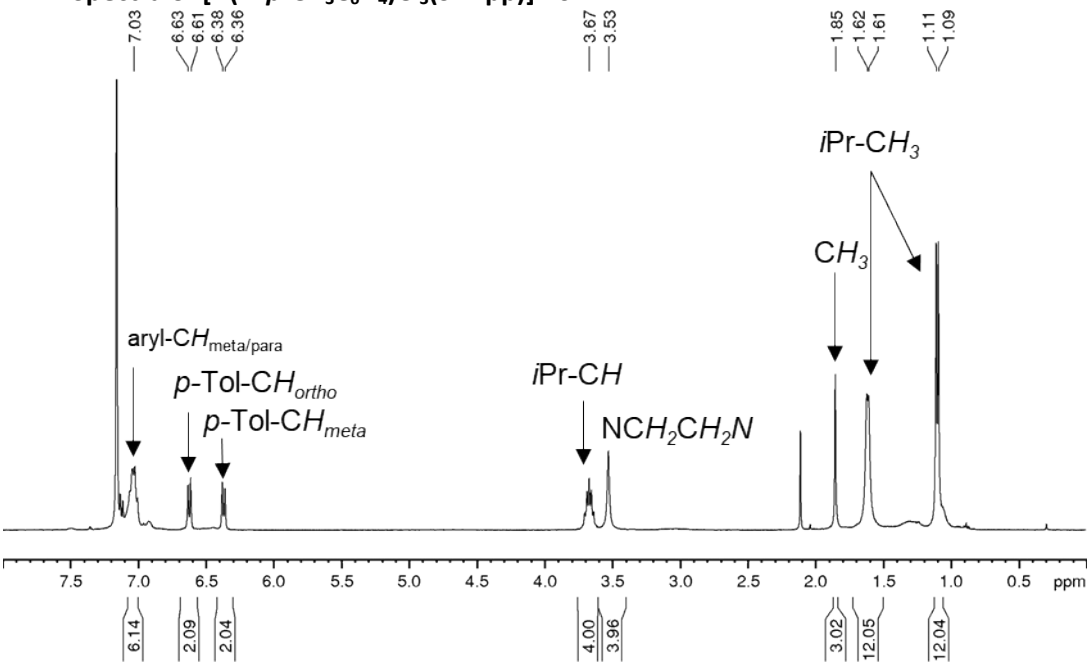

Figure S12: ^{1}H-NMR spectrum of [V(N-*p*-$CH_3C_6H_4$)Cl_3(SIDipp)] **16** in C_6D_6

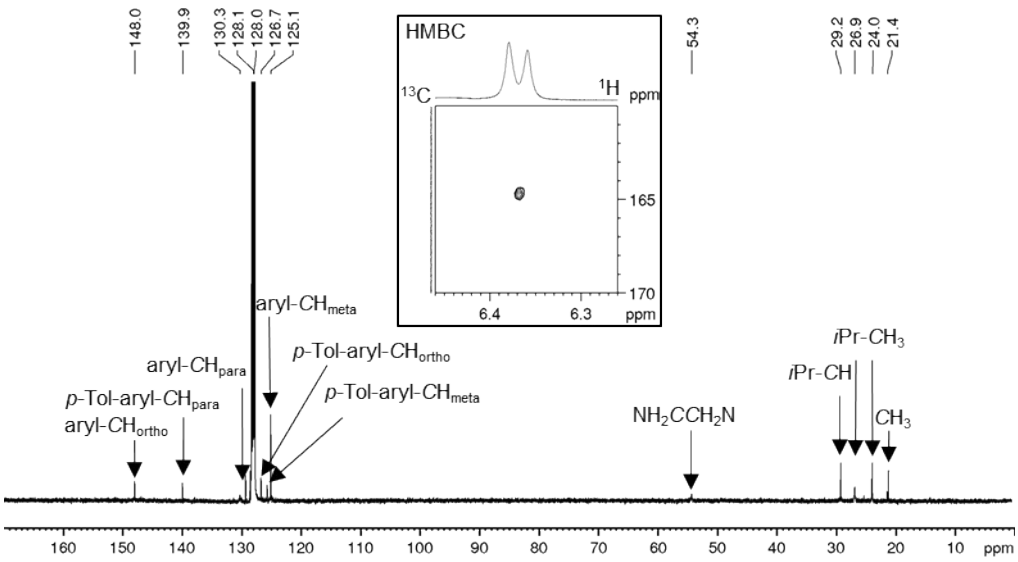

Figure S13: $^{13}C\{^1H\}$-NMR spectrum of [V(N-*p*-$CH_3C_6H_4$)Cl_3(SIDipp)] **16** in C_6D_6. The resonances for the aryl-C_{ipso} and the carbene carbon atom were not detected. One resonance at 127.8 ppm for (p-tolyl-aryl-C_{ortho}) coincides with the solvent signals.

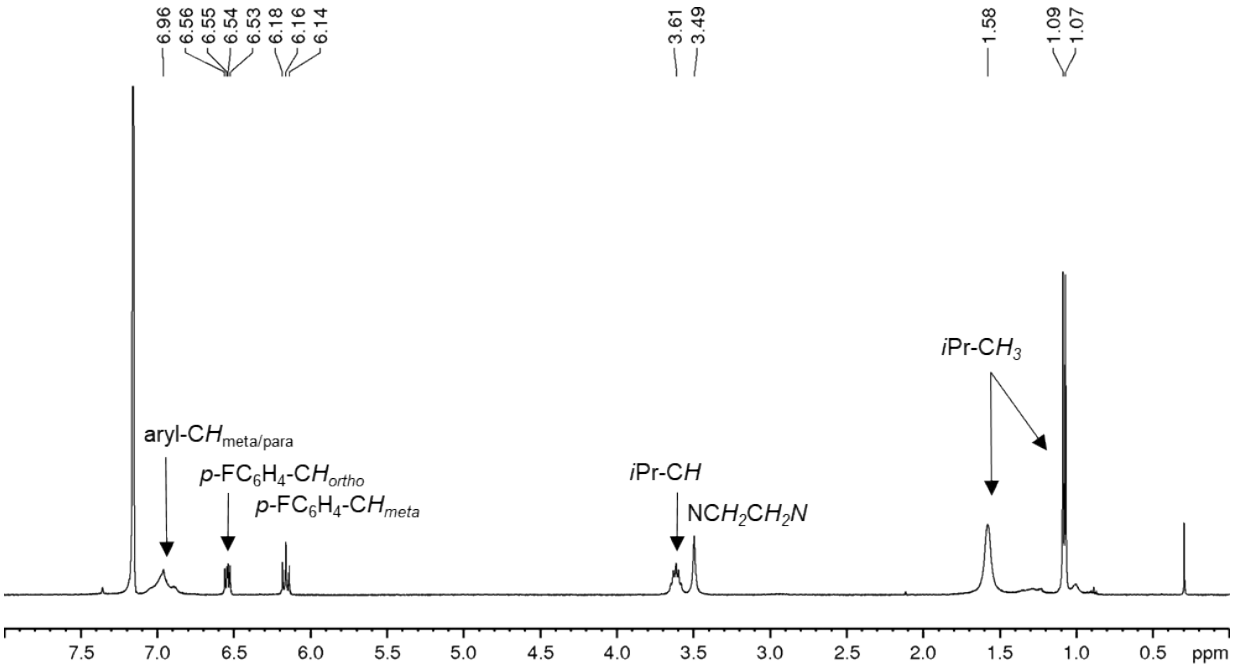

Figure S14: ^1H-NMR spectrum of [V(N-*p*-FC_6H_4)Cl_3(SIDipp)] **17** in C_6D_6.

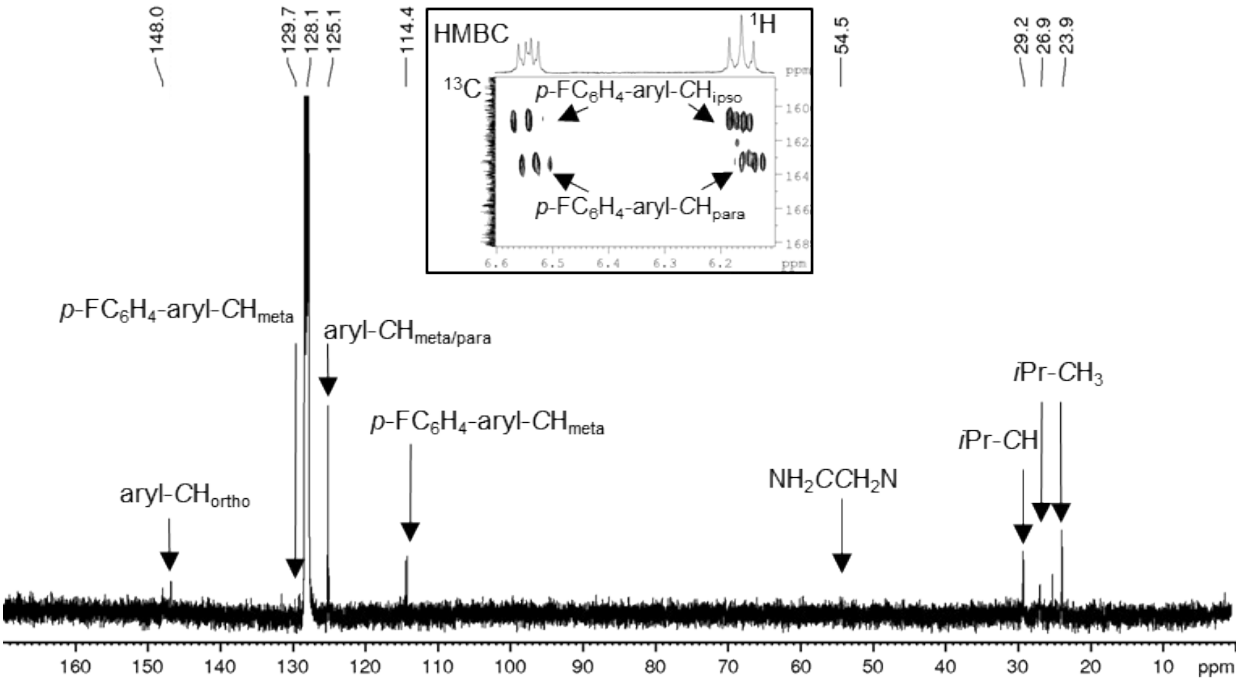

Figure S15: $^{13}C\{^{1}H\}$-NMR spectrum of [V(N-*p*-FC_6H_4)Cl_3(SIDipp)] **17** in C_6D_6. The resonance for the carbene carbon atom and the aryl-C_{ipso} were not detected.

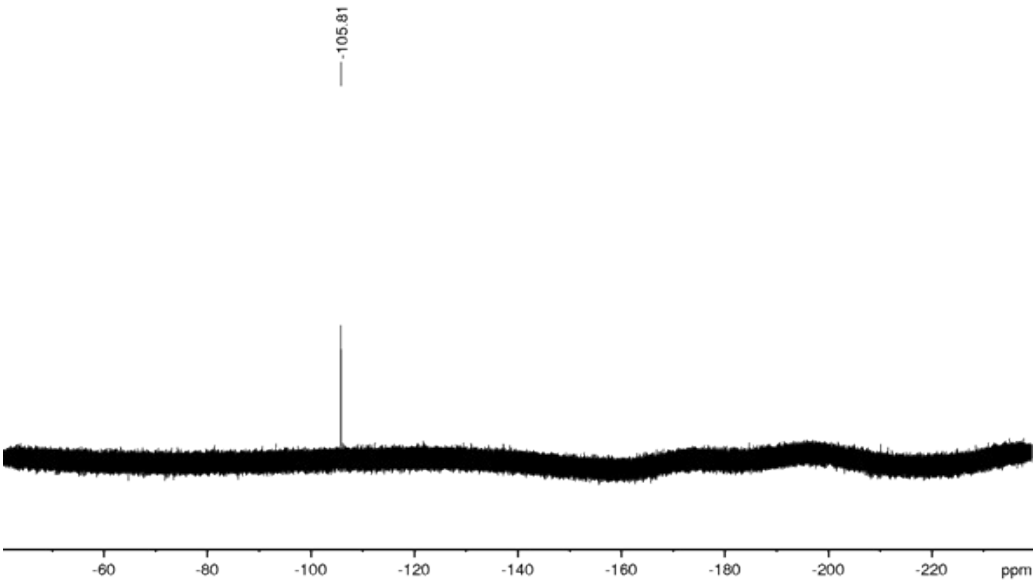

Figure S16: : $^{19}F\{^{1}H\}$ NMR spectrum of [V(N-*p*-FC_6H_4)Cl_3(SIDipp)] **17** in C_6D_6.

NMR Spectra of [V(N-*p*-$CH_3C_6H_4$)Cl_3(IMes)] 18

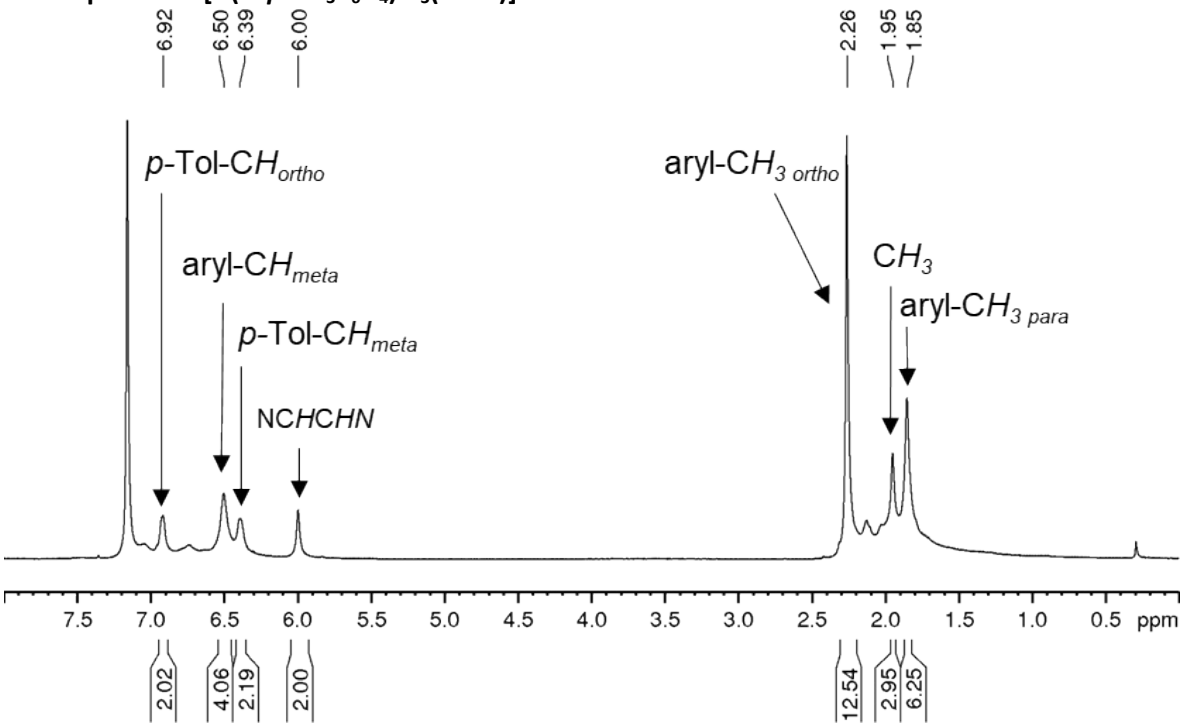

Figure S17:: ^{1}H-NMR spectrum of [V(N-*p*-$CH_3C_6H_4$)Cl_3(IMes)] **18** in C_6D_6.

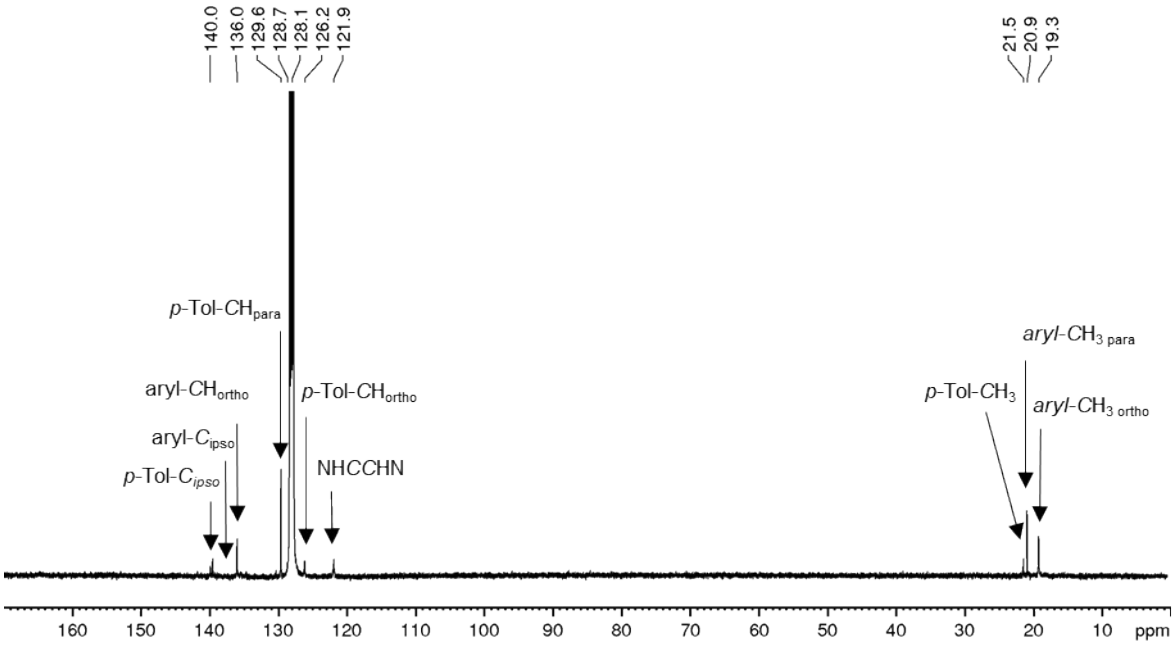

Figure S18: $^{13}C\{^1H\}$-NMR spectrum of [V(N-*p*-$CH_3C_6H_4$)Cl_3(IMes)] **18** in C_6D_6. The resonance for the carbene carbon atom could not be detected. Resonances at 128.0 ppm (aryl-C_{para}) and 128.7 ppm (*p*-Tol-) coincide with the solvent signals and were determined *via* HMBC.

NMR Spectra of [V(N-*p*-FC_6H_4)Cl_3(IMes)] 19

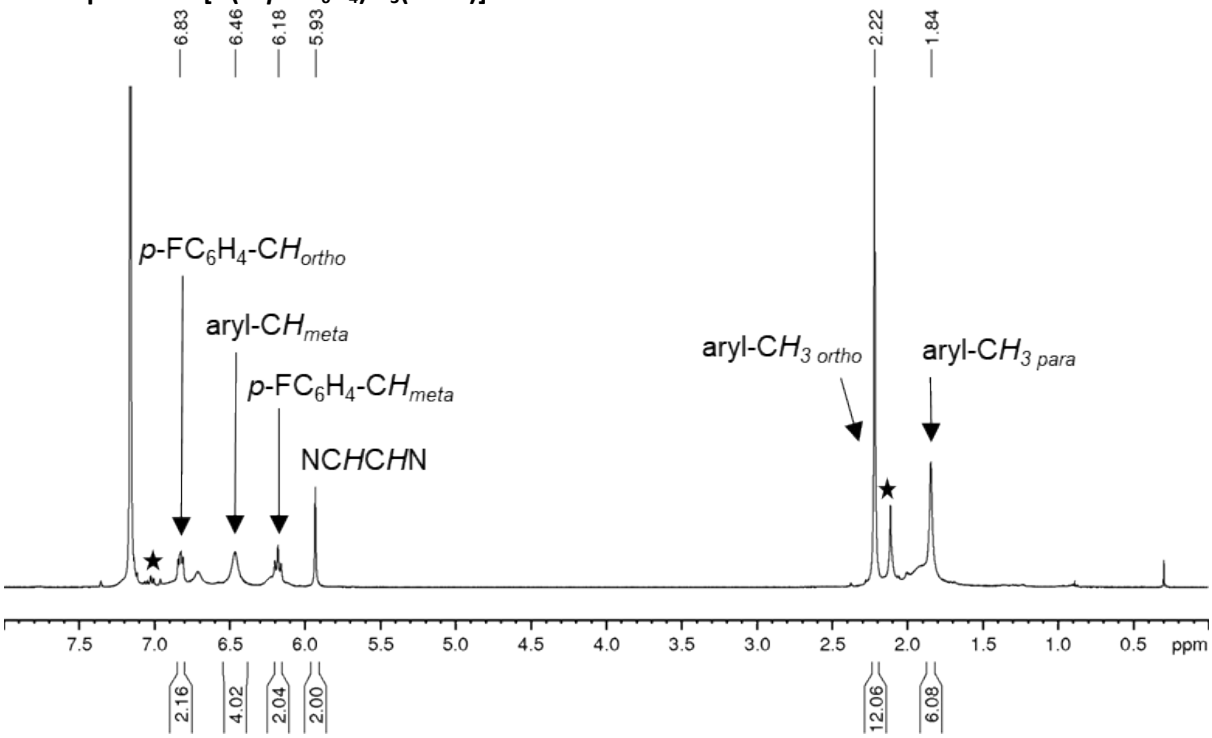

Figure S19: ^{1}H-NMR spectrum of [V(N-*p*-FC_6H_4)Cl_3(IMes)] **19** in C_6D_6. Residual traces of toluene are marked with a black asterisk.

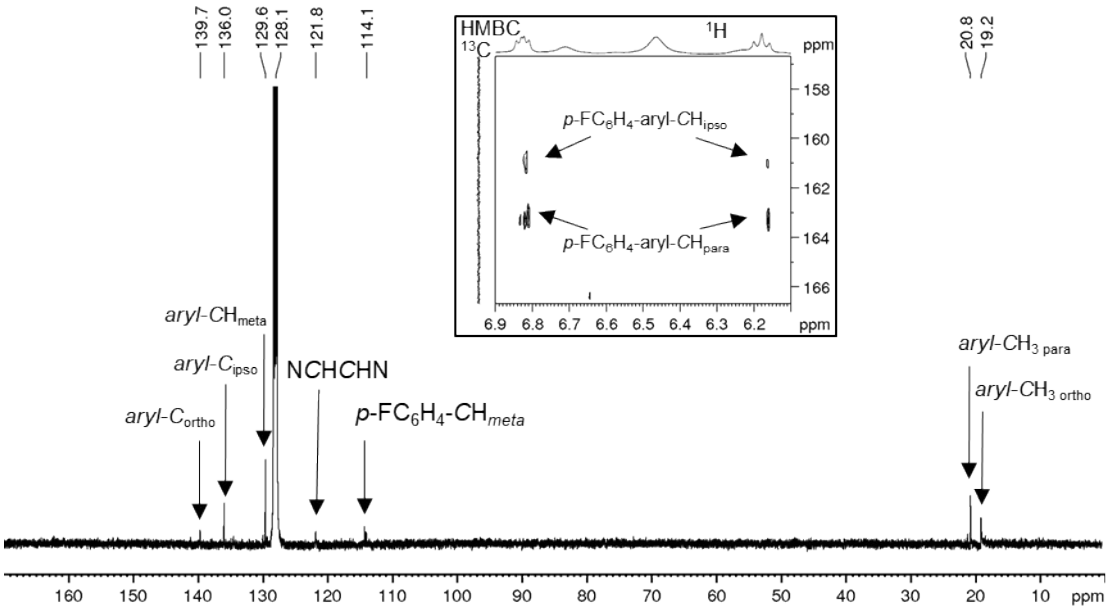

Figure S20: $^{13}C\{^1H\}$-NMR spectrum of [V(N-*p*-FC_6H_4)Cl_3(IMes)] **19** in C_6D_6.

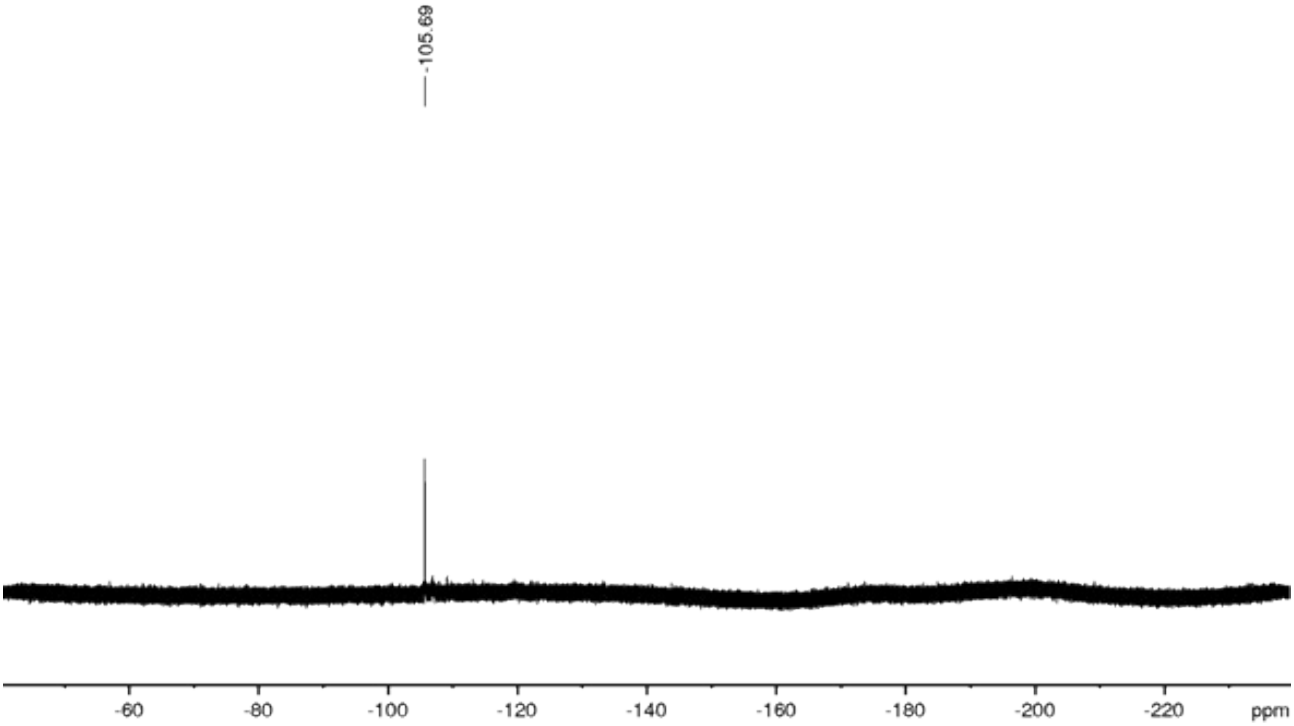

Figure S21: $^{19}F\{^{1}H\}$ NMR spectrum of [V(N-*p*-FC_6H_4)Cl_3(IMes)] **19** in C_6D_6.

NMR spectra of [(IPr)-*p*-$CH_3C_6H_4NCO$] 20

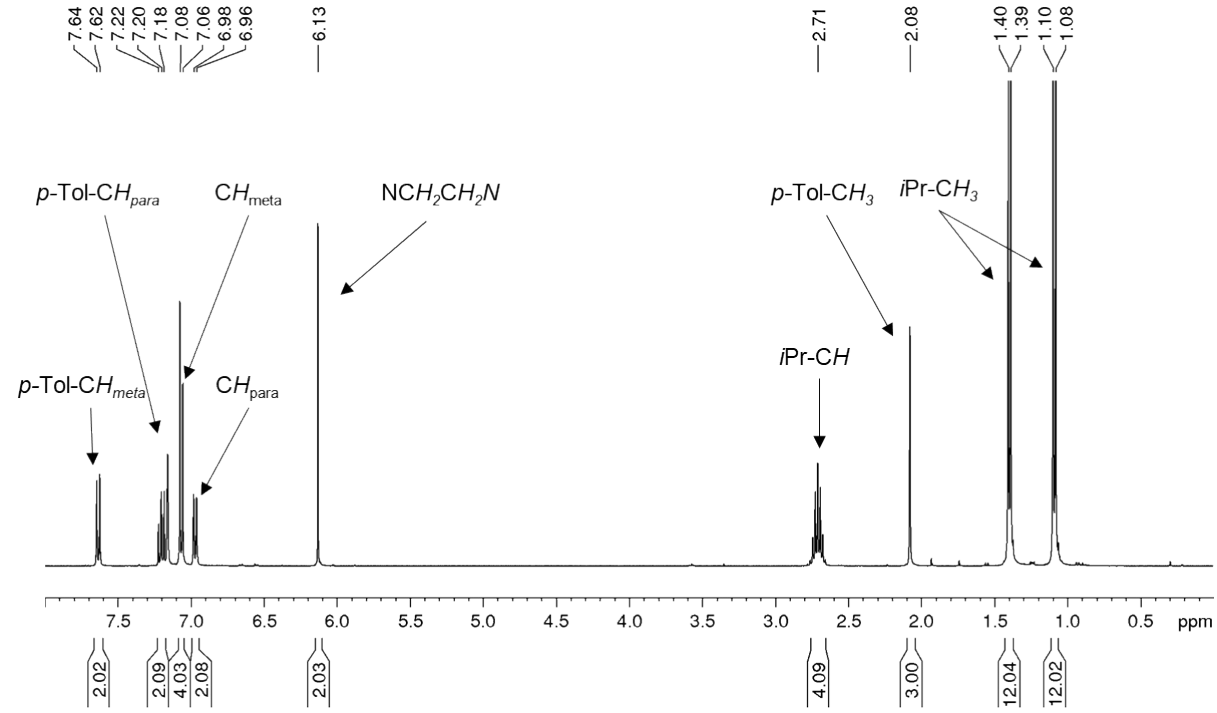

Figure S22: ^{1}H-NMR spectrum of [(IPr)- *p*-$CH_3C_6H_4NCO$] **20** in C_6D_6.

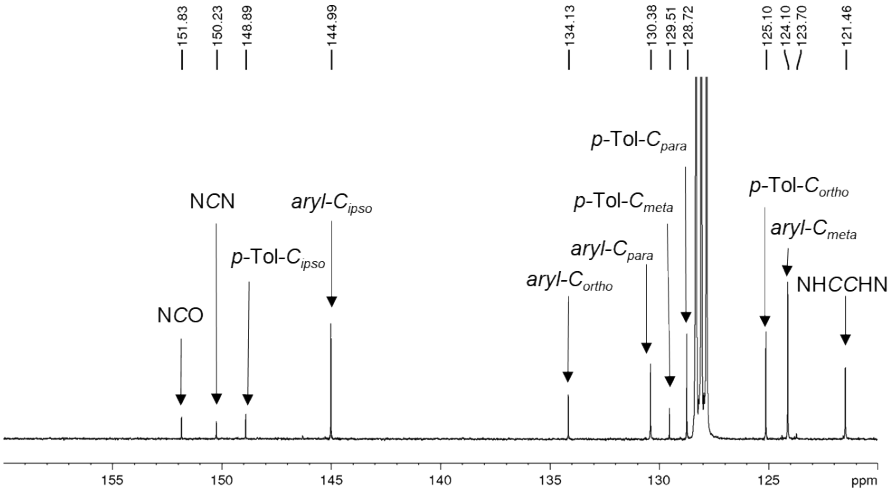

Figure S23: ^{13}C-NMR spectrum of [(IPr)- *p*-$CH_3C_6H_4NCO$] **20** in C_6D_6 (part 1).

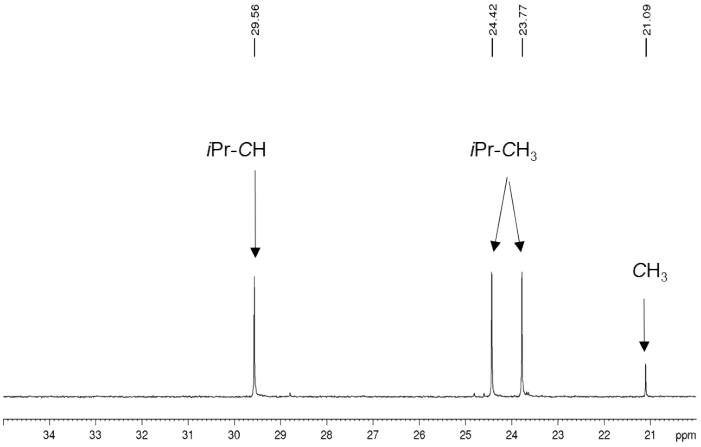

Figure S24: ^{13}C-NMR spectrum of [(IPr)- *p*-$CH_3C_6H_4NCO$] **20** in C_6D_6 (part 2).

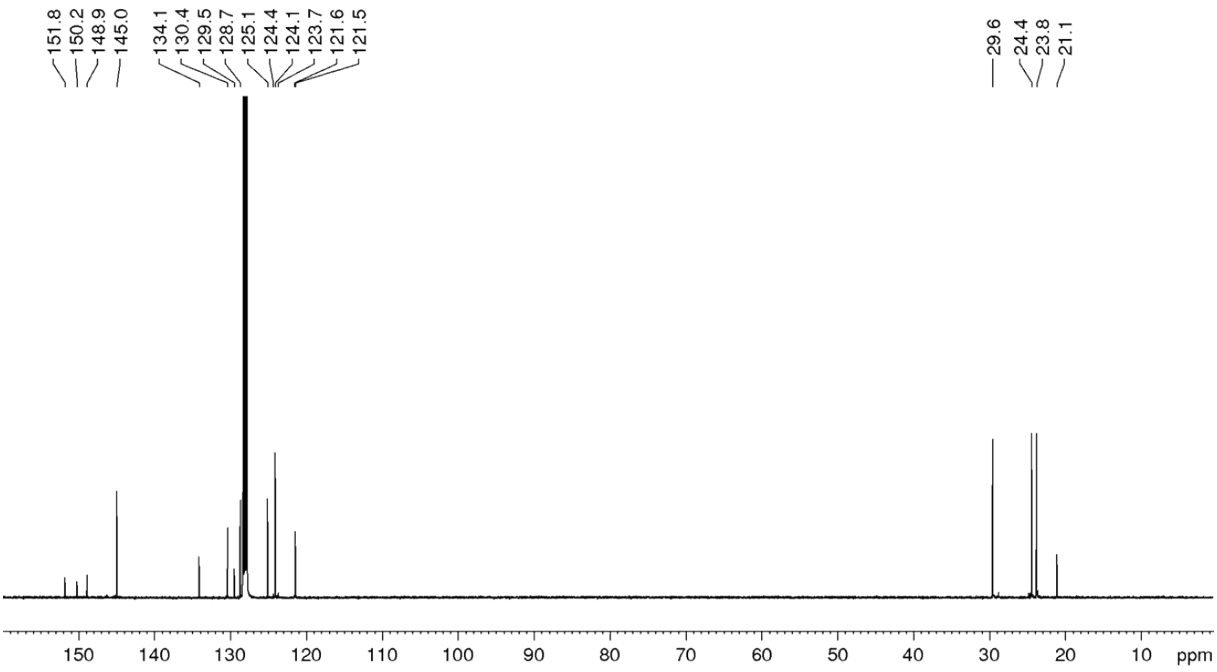

Figure S25: Full ^{13}C-NMR spectrum of [(IPr)- *p*-$CH_3C_6H_4NCO$] **20** in C_6D_6.

2) Crystal structures of the compounds

Crystal structure of [VCl_3(cAAC^{Me})] 1

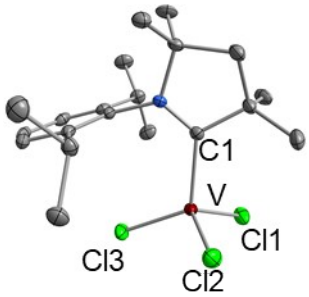

Figure S26: Molecular structure of [VCl_3(cAAC^{Me})] **1** in the solid state. Hydrogen atoms are omitted for clarity. Atomic displacement ellipsoids are set at 50 % probability. Selected bond lengths [Å] and angles [°] for **1**: V–C1 2.1179(13), V–Cl1 2.2195(3), V–Cl2 2.2042(5), V–Cl3 2.21122(5), N–C1 1.3029(16), C1-V-Cl1 98.83(4), C1-V-Cl2 105.73(4); C1-V-Cl3 117.72(4); Cl1-V-Cl2 114.254 (17), Cl2-V-Cl3 111.431(16), Cl3-V-Cl1 108.488(16).

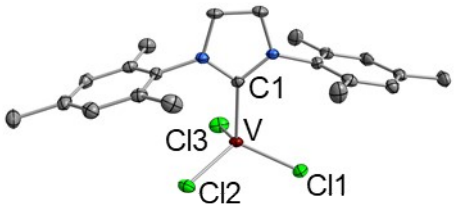

Crystal structure of [VCl_3(IMes)] 2

Figure S27: Molecular structure of [VCl_3(IMes)] **2** in the solid state. Hydrogen atoms are omitted for clarity. Atomic displacement ellipsoids are set at 50 % probability. Selected bond lengths [Å] and angles [°] for **2**: V–C1 2.112(3), V–Cl1 2.2142(9), V–Cl2 2.2098(9), V–Cl3 2.2084(10), C1-V-Cl1 107.99(8), C1-V-Cl2 108.86(8); C1-V-Cl3 104.51(9); Cl1-V-Cl2 110.62(4), Cl2-V-Cl3 111.32(4), Cl3-V-Cl1 113.23(4).

Crystal structure of [{VCl_2(I*i*Pr_2Me)(μ-Cl)}$_2$] 3

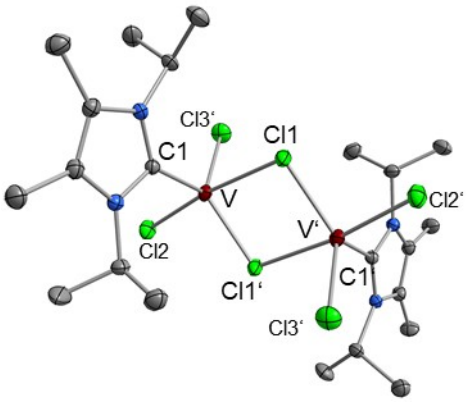

Figure S28: . Molecular structure of [{VCl_2(I*i*Pr_2Me)(μ-Cl)}$_2$] **3** in the solid state. Hydrogen atoms and a co-crystallized solvent molecule of toluene in **3** are omitted for clarity. Atomic displacement ellipsoids are set at 50 % probability. Selected bond lengths [Å] and angles [°] for **3**: V–C1/C1' 2.1191(20), V–Cl1/Cl1' 2.5362(6)/2.3282(6), V–Cl2/Cl2' 2.2454(6), V–Cl3/Cl3' 2.2630(6), C1-V-Cl1 83.76(5), C1-V-Cl1' 119.50(5), C1-V-Cl2 112.29(5), C1-V-Cl3 98.34(5), Cl1-V-Cl1' 79.168(9), Cl1-V-Cl2 172.71(2), Cl1'-V-Cl2' 88.43(2), Cl1'-V-Cl3 93.77(2), Cl3-V-Cl2 97.16(2).

Crystal structure of [VCl_3(IDipp)] 4

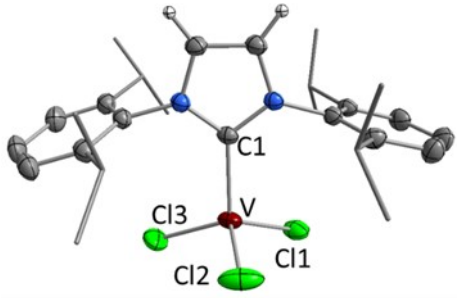

Figure S29: Molecular structure of [VCl_3(IDipp)] **4** in the solid state. Hydrogen atoms, except for the NHC backbone hydrogen atoms (idealized calculated positions; ball-stick model) are omitted for clarity. Atomic displacement ellipsoids are set at 50 % probability. Selected bond lengths [Å] and angles [°] for **4**: V–C1 2.1230(17), V–Cl1 2.2038(5), V–Cl2 2.2073(6), V–Cl3 2.2034(7), C1-V-Cl1 110.52(5), C1-V-Cl2 103.33(4), C1-V-Cl3 110.74(5), Cl1-V-Cl2 110.75(3), Cl2-V-Cl3 110.06(3), Cl3-V-Cl1 111.19(2).

Crystal structure of [VCl_3(SIDipp)] 5

Figure S30: Molecular structure of [VCl_3(SIDipp)] **5** in the solid state. Hydrogen atoms, except for the NHC backbone hydrogen atoms (idealized calculated positions; ball-stick model) are omitted for clarity. Atomic displacement ellipsoids are set at 50 % probability. Selected bond lengths [Å] and angles [°] for **5**: V–C1 2.1339(18), V–Cl1 2.2106(7), V–Cl2 2.2105(6), V–Cl3 2.2062(5), C1-V-Cl1 112.38(5), C1-V-Cl2 102.12(5); C1-V-Cl3 110.26(5); Cl1-V-Cl2 110.51(2), Cl2-V-Cl3 111.86(2), Cl3-V-Cl1 109.56(2).

Crystal structure of [$VCl_3(cAAC^{Me})_2$] 7

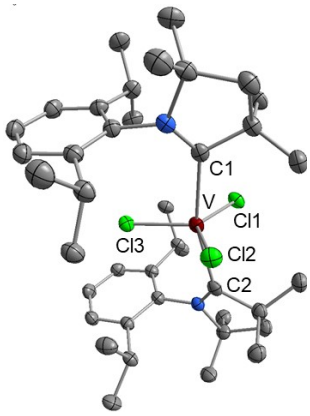

Figure S31: Molecular structure of [$VCl_3(cAAC^{Me})_2$] **7** in the solid state. Hydrogen atoms and 1.5 co-crystallized solvent molecules of benzene are omitted for clarity. Atomic displacement ellipsoids are set at 50 % probability. Selected bond lengths [Å] and angles [°] for **7**: V–C1 2.276(24), V–C2 2.2896(24), V–Cl1 2.2873(4), V–Cl2 2.2672(6), V–Cl3 2.2222(6), C1-V-C2 162.27(7), C1-V-Cl1 92.35(5), C1-V-Cl2 81.07(5), C1-V-Cl3 98.27(5), C2-V-Cl1 81.73(5), C2-V-Cl2 91.38(5), C2-V-Cl3 99.43(5), Cl1-V-Cl2 135.30(2); Cl2-V-Cl3 112.12(2), Cl3-V-Cl1 112.57(2).

Crystal structure of [VCl_3(I*i*PrMe)$_2$] 8

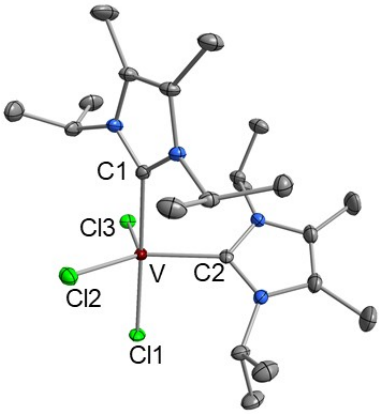

Figure S32: Molecular structure of Selected bond lengths [Å] and angles [°] for [VCl_3(I*i*PrMe)$_2$] **8** in the solid state. Hydrogen atoms are omitted for clarity. Atomic displacement ellipsoids are set at 50 % probability. Selected bond lengths [Å] and angles [°] for **8**: V–C1 2.255(2), V–C2 2.160(2), V–Cl1 2.3548(6), V–Cl2 2.2818(6), V–Cl3 2.2843(6), C1-V-C2 86.77(7), C1-V-Cl1 173.46(5), C1-V-Cl2 81.35(5), C1-V-Cl3 96.39(5), C2-V-Cl1 93.58(5), C2-V-Cl2 127.81(6), Cl2-V-Cl3 124.90(2), Cl3-V-C2 106.79(6) Cl1-V-Cl2 93.33(2), Cl1-V-Cl3 89.77(2).

Crystal structure of [VCl_3(cAAC^{Me})(THF)] 1(thf)

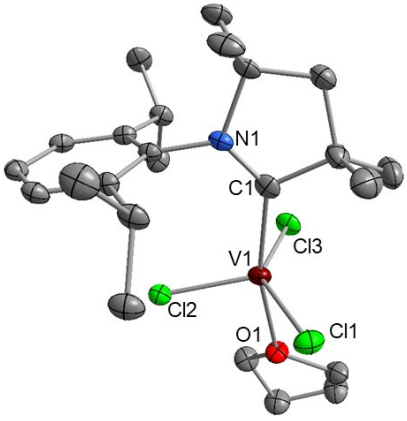

Figure S33: Molecular structure of [VCl_3(cAAC^{Me})(THF)] **1(thf)** in the solid state. Hydrogen atoms are omitted for clarity. Atomic displacement ellipsoids are set at 50 % probability. Selected bond lengths [Å] and angles [°] for **1(thf)**: C1–V1 2.1741(59), O1–V1 2.1921(45), Cl1–V1 2.2664(17), C1–N1 1.3107(79), Cl2–V1 2.2273(17), Cl3–V1 2.2630(16), C1-V1-O1 165.2(2), C1-V1-Cl1 91.55(17), C1-V1-Cl2 105.95(17), C1-V1-Cl3 88.34(17), Cl1-V1-Cl2 111.28(7), Cl2-V1-Cl3 109.61(7), Cl3-V1-Cl1 137.42(7), O1-V1-Cl1 83.71(12), O1-V1-Cl2 88.87(12), O1-V1-Cl3 85.74(13).

Crystal structure of [VCl_3(SIDipp)(THF)] 5(thf)

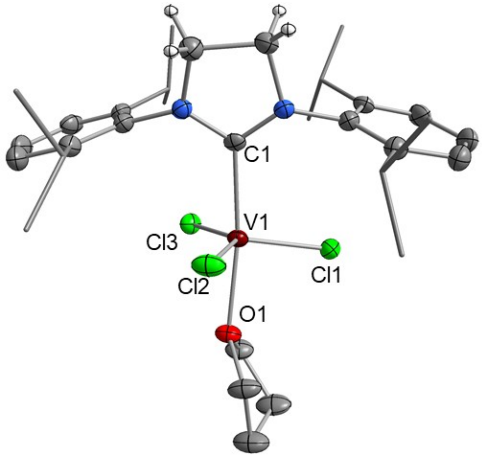

Figure S34: Molecular structure of [VCl_3(SIDipp)(THF)] **5(thf)** in the solid state. Hydrogen atoms are omitted for clarity. Atomic displacement ellipsoids are set at 50 % probability. Selected bond lengths [Å] and angles [°] for **5(thf)**: C1–V1 2.2129(33), O1–V1 2.1873(27), Cl1–V1 2.2298(10), Cl2–V1 2.2580(11), Cl3–V1 2.2386(10), C1-V1-O1 167.68(12), C1-V1-Cl1 102.95(9), C1-V1-Cl2 82.92(10), C1-V1-Cl3 97.42(9), O1-V1-Cl1 86.48(8), O1-V1-Cl2 85.66(8), O1-V1-Cl3 87.14(8), Cl1-V1-Cl2 117.85(4), Cl2-V1-Cl3 133.69(4), Cl3-V1-Cl1 107.23(4).

Crystal structure of [$MesVCl_2$($cAAC^{Me}$)] 9

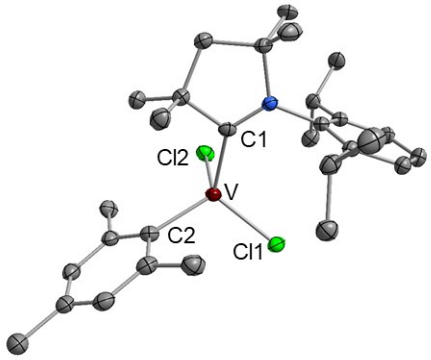

Figure S35: Molecular structure of [$MesVCl_2$($cAAC^{Me}$)] **9** in the solid state. Hydrogen atoms are omitted for clarity. Atomic displacement ellipsoids are set at 50 % probability. Selected bond lengths [Å] and angles [°] for **9**: V–C1 2.1281(18), V–C2 2.0779(23), V–Cl1 2.2367(4), V–Cl2 2.2369(6), N–C1 1.3071(24), C1-V-C2 114.77(7), C1-V-Cl1 112.97(5), C1-V-Cl2 93.03(5), C2-V-Cl1 109.69(5), C2-V-Cl2 112.41(5), Cl1-V-Cl2 113.20(2).

Crystal structure of $[cAAC^{Me}H]^+[VCl_2(Mes)_2]^-$ 10

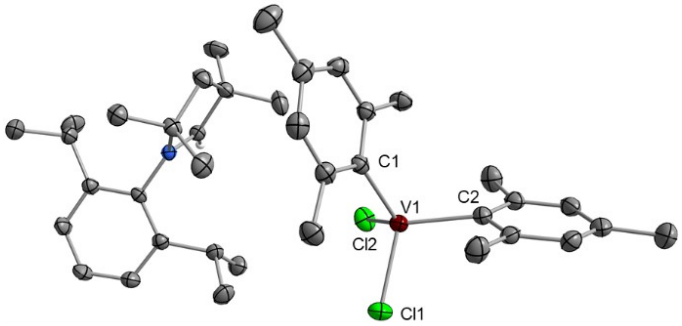

Figure S36: Molecular structure of $[cAAC^{Me}H]^+[VCl_2(Mes)_2]^-$ **10** in the solid state. Hydrogen atoms are omitted for clarity. Atomic displacement ellipsoids are set at 50 % probability. Selected bond lengths [Å] and angles [°] for **10**: C1–V1 2.0920(18), C2–V1 2.0895(23), Cl1–V1 2.2796(5), Cl2–V1 2.2856(6), C1-V1-C2 109.43(17), C1-V1-Cl1 116.86(5), C1-V1-Cl2 108.19(5), C2-V1-Cl1 106.32(5), C2-V1-Cl2 117.83(6), Cl1-V1-Cl2 98.23(2).

Crystal structure of $[(NPh_2)VCl_2(cAAC^{Me})]$ 11

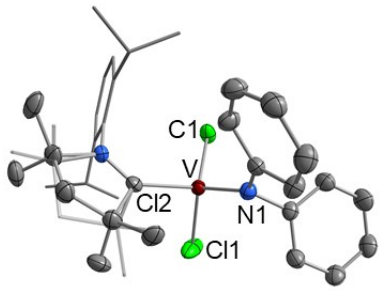

Figure S37: Molecular structure of $[(NPh_2)VCl_2(cAAC^{Me})]$ **11** in the solid state. Hydrogen atoms are omitted for clarity. Atomic displacement ellipsoids are set at 50 % probability. Selected bond lengths [Å] and angles [°] for **11** (the five membered ring of the $cAAC^{Me}$-ligand showed disorder in the CH_2 position and is also displayed): V–C1 2.1411(21), V–N1 1.8832(15), V–Cl1 2.2625(5), V–Cl2 2.2258(6), C1-V-N1 106.28(6), C1-V-Cl1 102.48(5), C1-V-Cl2 113.01(5), N1-V-Cl1 110.75(5), N1-V-Cl2 109.66(5), Cl1-V-Cl2 114.23(3).

Crystal structure of [V(O)Cl_3(IDipp)] 12

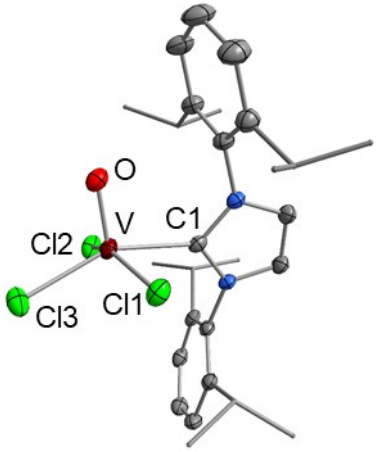

Figure S38: Molecular structure of [V(O)Cl_3(IDipp)] **12** in the solid state. Hydrogen atoms are omitted for clarity. Atomic displacement ellipsoids are set at 50 % probability. Selected bond lengths [Å] and angles [°] for **12**: V–C1 2.1582(13), V–O 1.566(1), V–Cl1 2.2405(5), V–Cl2 2.2164(5), V–Cl3 2.2628(5), C1-V-O 100.00(5), C1-V-Cl1 79.39(4), Cl1-V-Cl2 152.411(17); C1-V-Cl3 153.14(4), Cl1-V-Cl3 90.481(16), Cl3-V-Cl2 92.865(16), Cl3-V-C1 85.46(4), O-V-Cl1 102.68(4), O-V-Cl2 102.57(4), O-V-Cl3 106.51(4).

Crystal structure of [V(O)Cl_3(SIDipp)] 13

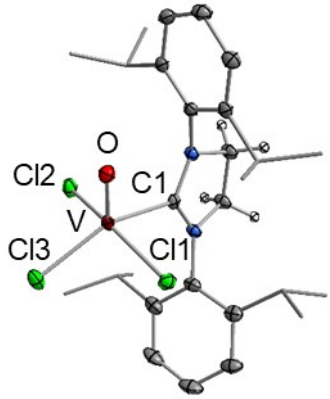

Figure S39: Molecular structure of [V(O)Cl_3(SIDipp)] **13** in the solid state. Hydrogen atoms, except for the backbone hydrogen atoms in **13** (stick and ball representation), are omitted for clarity. Atomic displacement ellipsoids are set at 50 % probability. Selected bond lengths [Å] and angles [°] for **13**: V–C1 2.1658(13), V–O 1.5702(11), V–Cl1 22178(4), V–Cl2 2.2216(4), V–Cl3 2.2542(5), C1-V-O 101.40(5), C1-V-Cl1 84.25(4),C1-V-Cl2 78.36(4), Cl1-V-Cl2 152.589(17); C1-V-Cl3 148.91(4), Cl1-V-Cl3 91.814(15), Cl3-V-Cl2 92.283(15), Cl3-V-C1 78.36(4), O-V-Cl1 101.86(4), O-V-Cl2 102.23(4), O-V-Cl3 109.57(4).

Crystal structure of [V(N-*p*-$CH_3C_6H_4$)Cl_3(IMes)] 18

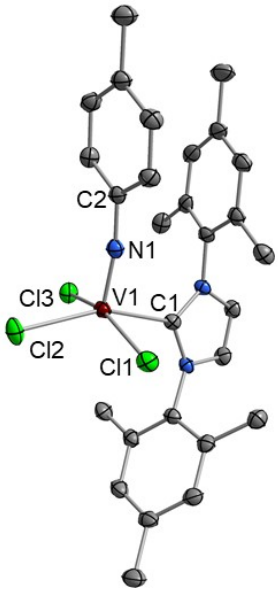

Figure S40: Molecular structure of [V(N-*p*-$CH_3C_6H_4$)Cl_3(IMes)] **18** Atomic displacement ellipsoids are set at 50 % probability. Selected bond lengths [Å] and angles [°] for [V(N-*p*-$CH_3C_6H_4$)Cl_3(IMes)] **18**: C1–V1 2.1666(18), V1–N1 1.6371(15), V1–Cl1 2.2602(5), V1–Cl2 2.2710(6), V1–Cl3 2.2790(5), N1–C2 1.3816(22), C1-V1-N1 99.80(7), C1-V1-Cl1 85.89(4), C1-V1-Cl2 153.95(5), C1-V1-Cl3 81.34(4), Cl1-V1-Cl2 92.805(19), Cl1-V1-Cl3 156.16(2), Cl2-V1-Cl3 89.988(19), V1-N1-C2 171.31(13).

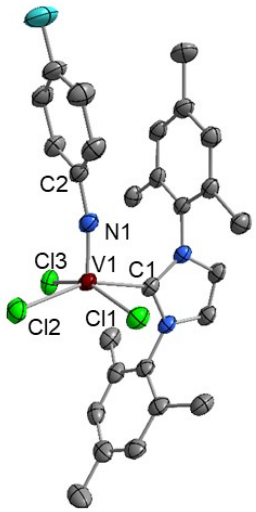

Crystal structure of [V(N-*p*-FC_6H_4)Cl_3(IMes)] 19

Figure S41: Molecular structure of [V(N-*p*-FC_6H_4)Cl_3(IMes)] **19** in the solid state. Hydrogen atoms and a cocrystallized solvent molecule of benzene are omitted for clarity. Atomic displacement ellipsoids are set at 50 % probability. Selected bond lengths [Å] and angles [°] for [V(N-*p*-FC_6H_4)Cl_3(IMes)] **19**: C1–V1 2.1541(17), V1–N1 1.6338(15), V1–Cl1 2.2715(5), V1–Cl2 2.2937(6), V1–Cl3 2.2425(6), N1–C2 1.3860(21), C1-V1-N1 99.58(7), C1-V1-Cl1 82.40(5), C1-V1-Cl2 157.07(5), C1-V1-Cl3 88.24(5), Cl1-V1-Cl2 88.139(19), Cl1-V1-Cl3 154.36(2), Cl2-V1-Cl3 91.47(2), V1-N1-C2 167.20(13).

Crystal structure of [(IDipp)-*p*-TolNCO] 20

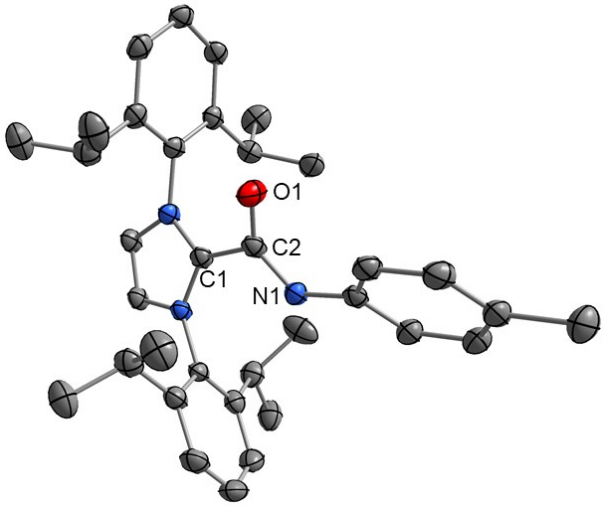

Figure S42: Molecular structure of [(IDipp)-*p*-TolNCO] **20** in the solid state. Hydrogen atoms are omitted for clarity. Atomic displacement ellipsoids are set at 50 % probability. Selected bond lengths [Å] and angles [°] for **20**: C1–C2 1.5161(18), C2–N1 1.3069(18), C2–O1 1.2530(17), C1-C2-O1 115.97(12), O1-C2-N1 134.10(13), N1-C2-C1 109.87(12).

3) UV-VIS Spectra of [VCl_3(cAAC^{Me})] 1 , [VCl_3(IMes)] 2, their oxidized forms and [VCl_3(cAAC^{Me})$_2$] 7

UV-VIS Spectra of [VCl_3(cAAC^{Me})] 1 and [$V(O)Cl_3$(cAAC^{Me})]

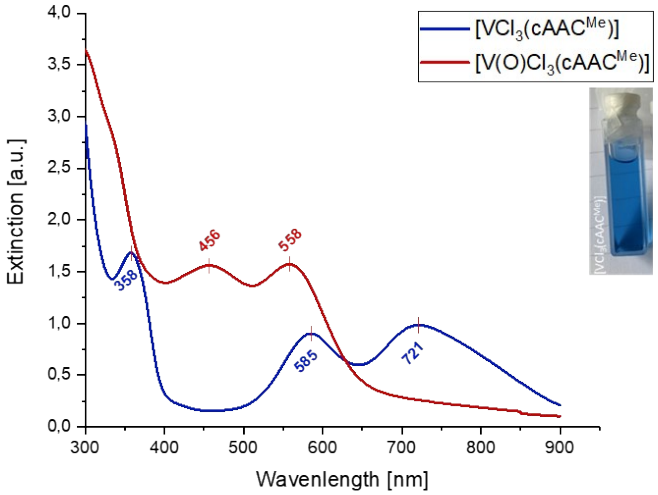

Figure S43: UV-VIS Spectra of [VCl_3(cAAC^{Me})] **1** (blue) and its oxidized form [$V(O)Cl_3$(cAAC^{Me})] (red) in toluene at room temperature. Molar-extinction-coefficients of 1: ε_{358}= 664 L·mol^{-1}cm^{-1}, ε_{721}= 387 L·mol^{-1}cm^{-1}, ε_{358}= 664 L·mol^{-1}cm^{-1}. Molar-extinction-coefficients of oxidized form: ε_{456}= 616 L·mol^{-1}cm^{-1}, ε_{558}= 620 L·mol^{-1}cm^{-1}.

UV-VIS Spectra of [VCl_3(IMes)] 2 and [$V(O)Cl_3$(IMes)]

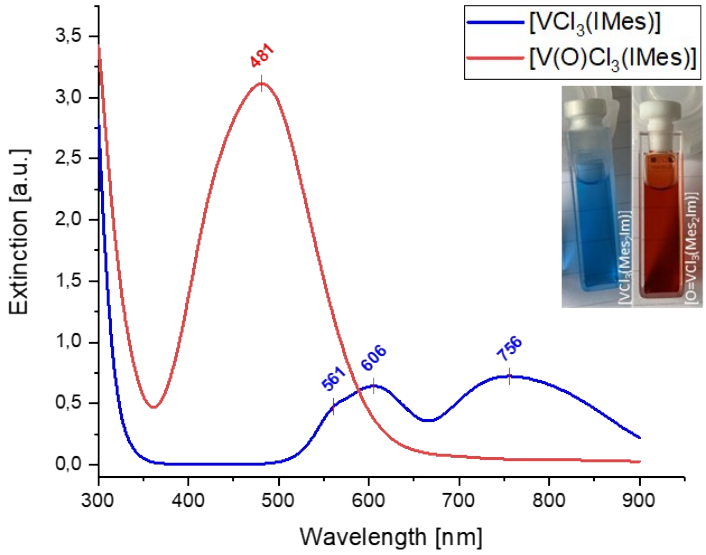

Figure S44: UV-VIS Spectra of [VCl_3(IMes)] **2** (blue) and its oxidized form [$V(O)Cl_3$(IMes)] (red) in toluene at room temperature. Molar-extinction-coefficients of **2**: ε_{561}= 234 L·mol^{-1}cm^{-1}, ε_{606}= 317 L·mol^{-1}cm^{-1}, ε_{756}= 357 L·mol^{-1}cm^{-1}. Molar-extinction-coefficients of oxidized form: ε_{481}= 1540 L·mol^{-1}cm^{-1} (CT-transition).

UV-VIS Spectra of $[VCl_3(cAAC)_2]$ 7

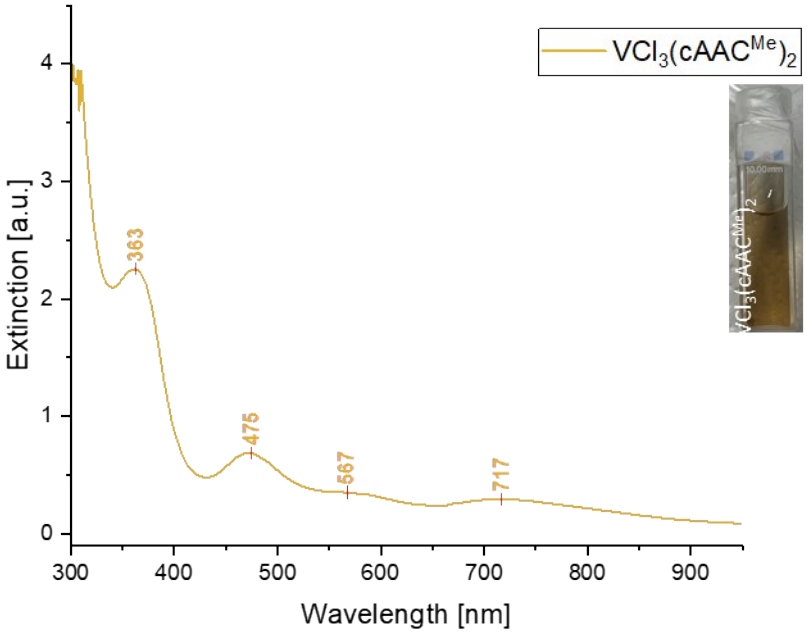

Figure S45: UV-VIS Spectra of $[VCl_3(cAAC^{Me})_2]$ **7** (orange) in toluene at room temperature. Molar-extinction-coefficients of **7** 363 (ε = 939 $Lmol^{-1}cm^{-1}$), 475 (ε = 287 $Lmol^{-1}cm^{-1}$), 567 (ε = 145 $Lmol^{-1}cm^{-1}$), 717 (ε = 123 $Lmol^{-1}cm^{-1}$).

4) EPR Experimental Data

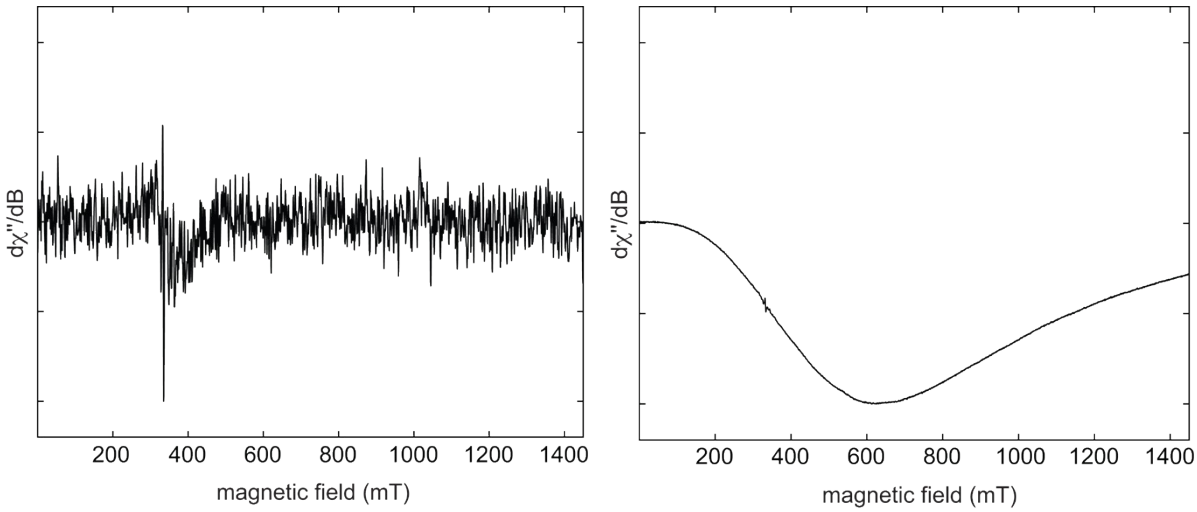

Figure S46: Experimental X-band CW EPR spectra of a powder sample of [VCl_3(cAAC^{Me})] **1** at room temperature (left) and 70 K (right).

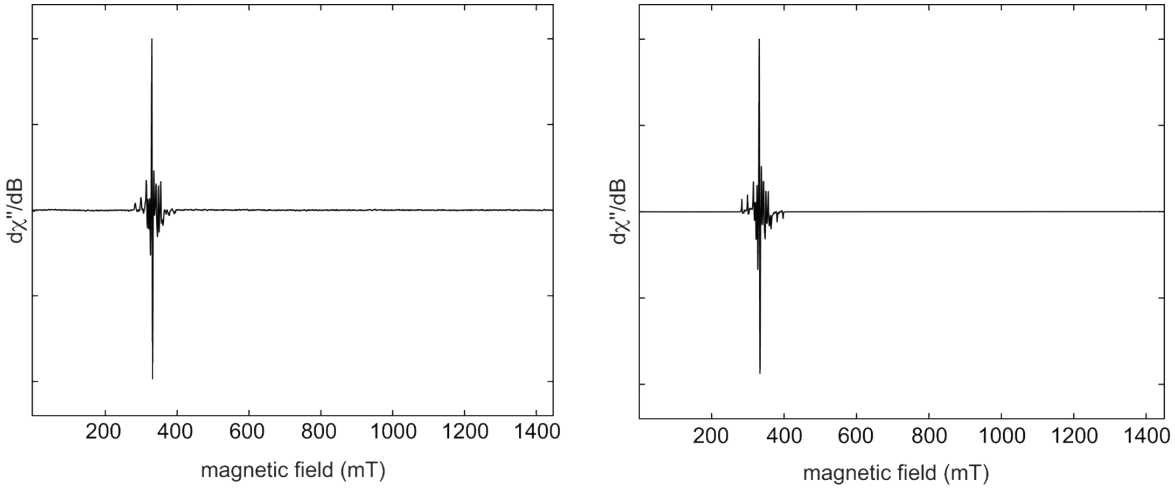

Figure S47: Experimental X-band CW EPR spectra of a microcrystalline sample of [VCl_3(cAAC^{Me})$_2$] **7** at room temperature (left) and 70 K (right). The detected resonances can be assigned to d^1 impurities of the air-sensitive compound **7** (for more details see Figure S45 provided in the SI).

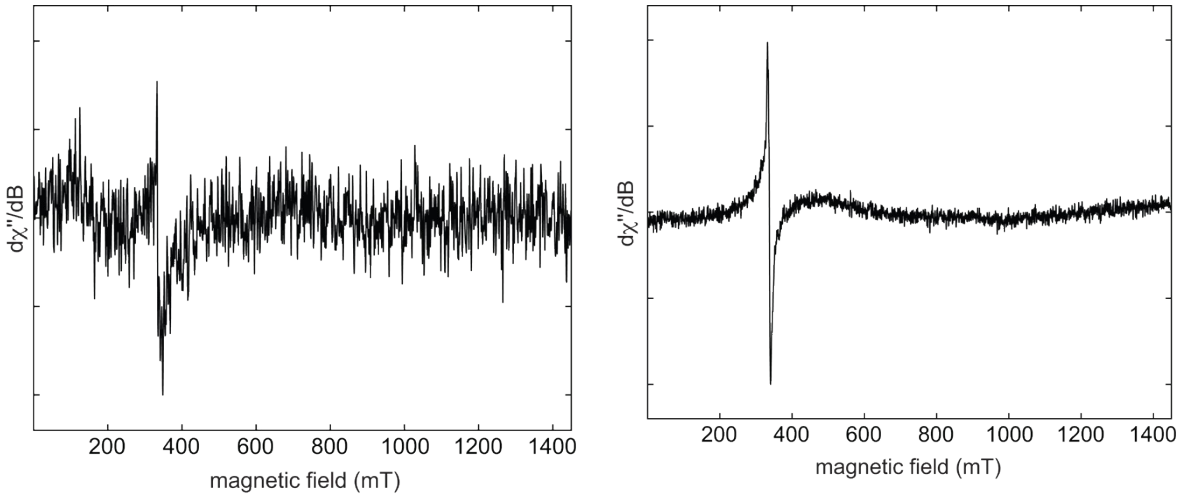

Figure S48: Experimental X-band CW EPR spectra of a microcrystalline sample of [VCl_3(IMes)] **2** at room temperature (left) and 70 K (right).

In the absence of resolved features of zero-field splitting, the X-band CW EPR spectra of the vanadium complexes show only resonances for vanadium *S* = 1/2 impurities at room temperature and 70 K (see Figure S46 in the SI). Only in the case of [VCl_3(cAAC^{Me})] (Figure S46), a broad baseline observed at 70 K might indicate the presence of electron-electron couplings expected for a *S* = 1 spin state. As the zero field parameters in the solid state are not resolved by X-band EPR measurements, we also conducted EPR experiments of [VCl_3(cAAC^{Me})] (**1**), [VCl_3(IMes)] (**2**), [VCl_3(IDipp)] (**4**) and [VCl_3(cAAC^{Me})$_2$] (**7**) in solution. Again, only resonances associated with d^1 impurities were detected (see Figure S49).

We also conducted a series of EPR experiments in toluene solutions of [VCl_3(cAAC^{Me})] (**1**), [VCl_3(IMes)] (**2**), [VCl_3(IPr)] (**4**) and [VCl_3(cAAC^{Me})$_2$] (**7**). The compounds were either crystallized from a saturated solution in toluene at -80°C ([VCl_3(cAAC^{Me})] (**1**) and [VCl_3(IPr)] (**4**)), sublimed ([VCl_3(IMes)] (**2**)) or recrystallized from *n*-hexane ([VCl_3(cAAC^{Me})$_2$] **7**) prior to dissolution in dry toluene.

For [VCl_3(IPr)] (**4**), only ^{51}V hyperfine couplings (*I* = 7/2, 99.75% natural abundance) of a d^1 impurity were resolved at 293 K and a typical octet-splitting pattern was detected, as depicted in Figure SI45 (a). Similar EPR spectra were observed for comparable vanadium complexes.[1] Frozen solution EPR spectra, recorded at 70 K, revealed the corresponding anisotropic parameters for the d^1 impurities in the mono NHC complex [VCl_3(IMes)] (**2**), the mono- and bis cAAC^{Me} stabilized complexes [VCl_3(cAAC^{Me})] (**1**) and [VCl_3(cAAC^{Me})$_2$] (**7**) (see Figure S45). Apart from these resonances, no further signals could be observed in a full magnetic field sweep.

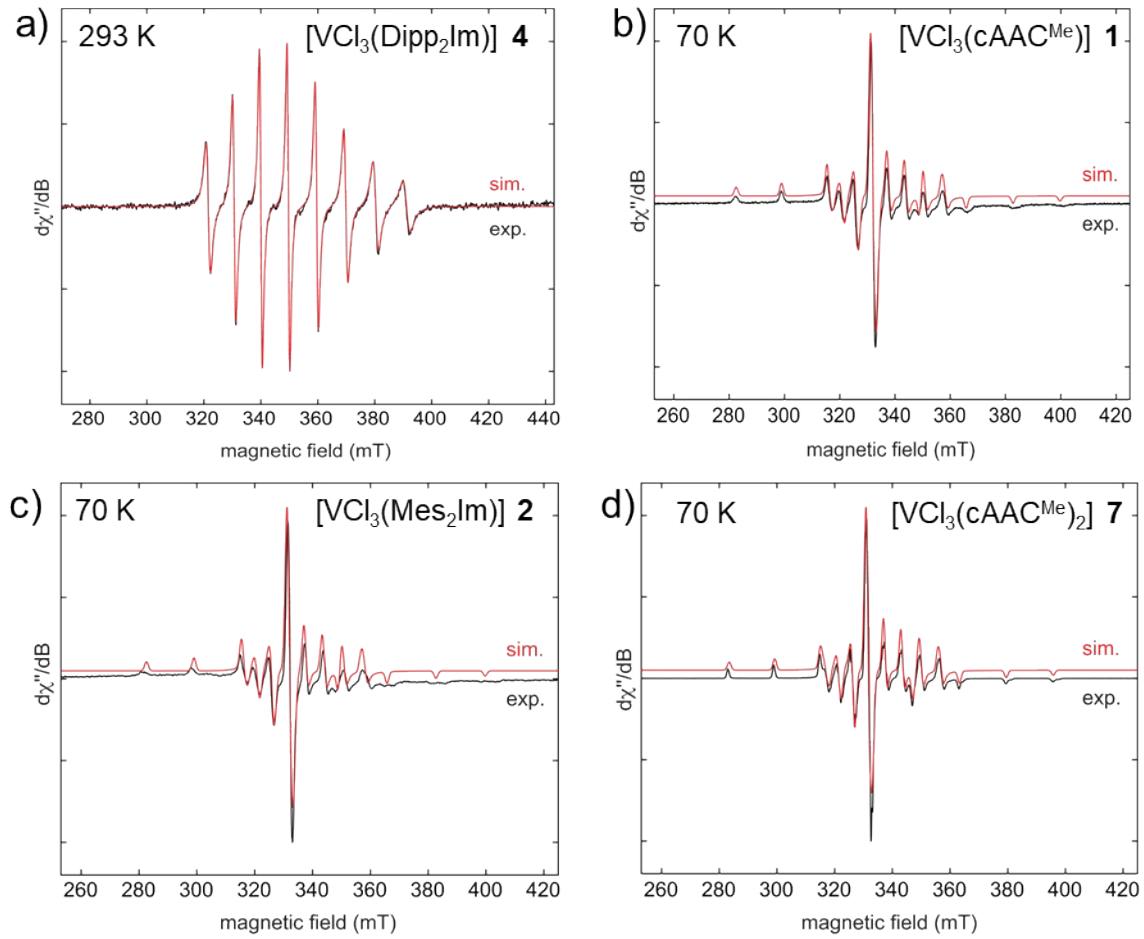

Figure S49: (a) Experimental (black) and simulated (red) X-band CW-EPR spectrum of [VCl_3(IDipp)] **4** (top left) dissolved in toluene at 293 K. The simulation leads to an orthorhombic g tensor (g_1 = 1.99, g_2 = 1.96, g_3 = 1.97), vanadium hyperfine couplings of $A(^{51}V)$ = 231, 255, and 343 MHz, and a rotational correlation time (τ_r) of 0.5 ns. (b) Experimental (black) and simulated (red) X-band CW-EPR spectrum of [VCl_3(cAAC^{Me})] **1** (top right) in frozen toluene at 70 K. The simulation leads to an axial g tensor ($g_\perp$= 1.983, $g_\parallel$ = 1.964) and vanadium hyperfine couplings of $A_\perp(^{51}V)$ = 161 MHz and $A_\parallel(^{51}V)$ = 460 MHz. The full spectrum shows no additional features, meaning the baseline remains flat at 70 K. (c) Experimental (black) and simulated (red) X-band CW-EPR spectrum of [VCl_3(IMes)] **2** (bottom left) in frozen toluene solution at 70 K. Simulation leads to an axial g tensor ($g_\perp$= 1.983, $g_\parallel$ = 1.964) and vanadium hyperfine couplings of $A_\perp(^{51}V)$ = 161 MHz and $A_\parallel(^{51}V)$ = 460 MHz. The full spectrum shows no additional features, meaning the baseline remains flat at 70 K. (d) Experimental (black) and simulated (red) X-band CW-EPR spectrum of [VCl_3(cAAC^{Me})$_2$] **7** (bottom right) in frozen toluene at 70 K (*black*). Simulation (*red*) leads to an axial g tensor ($g_\perp$= 1.985, $g_\parallel$ = 1.973) and vanadium hyperfine couplings of $A_\perp(^{51}V)$ = 154 MHz and $A_\parallel(^{51}V)$ = 443 MHz. The full spectrum shows no additional features, meaning the baseline remains flat at 70 K.

5) Computational details – optimized geometries

Calculations have been performed using the TURBOMOLE V7.2 program suite, a development of University of Karlsruhe and the Forschungszentrum Karlsruhe GmbH, 1989-2007, TURBOMOLE GmbH, since 2007; available from http://www.turbomole.com.[2] Geometry optimizations were performed using (RI-)DFT calculations[3] on a m4 grid employing the D3BJ[4] dispersion-corrected PBE0[5] functional and a def2-TZVP basis set for vanadium and for all other atoms the def2-SVP basis sets.[6] Vibrational frequencies were calculated at the same level with the AOFORCE[7] module and all structures represented true minima without imaginary frequencies.

Cartesian coordinated of the complexes

ax,ax-[VCl_3(l*i*Pr)$_2$]
Energy = -3246.259574 h

V	-0.4997386	-0.3995759	-0.0114592
Cl	1.7361376	-0.3997538	-0.5135899
Cl	-1.7546157	1.4903443	0.1678698
Cl	-1.7424058	-2.2968182	0.1720594
C	-0.6107217	-0.3978165	-2.2567744
N	-0.6147102	0.6737150	-3.0934349
N	-0.6197939	-1.4657351	-3.0978934
C	-0.6662318	0.2838344	-4.4148397
C	-0.3943166	2.0711529	-2.7115310
C	-0.6694542	-1.0701062	-4.4176705
C	-0.4064281	-2.8657673	-2.7216854
H	-0.6901533	0.9920452	-5.2375128
H	-0.3136363	2.0604228	-1.6202654
C	-1.5882502	2.9323943	-3.0853313
C	0.9252249	2.5682249	-3.2840857
H	-0.6967054	-1.7747761	-5.2432706
H	-0.3228803	-2.8593463	-1.6306277
C	0.9088060	-3.3682748	-3.2993687
C	-1.6061823	-3.7188691	-3.0954752
H	-1.4271113	3.9643919	-2.7410215
H	-1.7494389	2.9631214	-4.1750609
H	-2.4969810	2.5493133	-2.6005540
H	0.9093756	2.6206039	-4.3843484
H	1.1357451	3.5790956	-2.9050951
H	1.7475547	1.9062717	-2.9759246
H	1.1148731	-4.3813581	-2.9238685
H	0.8898616	-3.4173895	-4.3997358
H	1.7355919	-2.7117436	-2.9914955
H	-2.5114676	-3.3327781	-2.6066306
H	-1.7706997	-3.7443494	-4.1848501
H	-1.4498282	-4.7530892	-2.7556531
C	-0.3983892	-0.3956557	2.2545872
N	-1.4962936	-0.3989562	3.0612585
N	0.6413786	-0.3897209	3.1305702
C	-1.1459801	-0.3953601	4.3921170
C	-2.9044177	-0.4047998	2.6468492
C	0.2074273	-0.3894997	4.4381578
C	2.0644993	-0.3831538	2.7904272
H	-1.8786792	-0.3972282	5.1932624
H	-2.8875692	-0.4065721	1.5527795
C	-3.6003703	0.8643376	3.1124468
C	-3.5912307	-1.6773161	3.1167268
H	0.8867709	-0.3852045	5.2850512
H	2.0965557	-0.3846285	1.6956412
C	2.7418355	-1.6499806	3.2892878
C	2.7293054	0.8915559	3.2861086
H	-4.6284750	0.8856432	2.7224824
H	-3.6579641	0.9253025	4.2110694
H	-3.0716022	1.7488910	2.7316549
H	-3.6482606	-1.7350356	4.2155480
H	-4.6192084	-1.7072205	2.7269916

H	-3.0562533	-2.5593846	2.7388405
H	3.7842936	-1.6763474	2.9398634
H	2.7556922	-1.7099604	4.3895642
H	2.2288262	-2.5415549	2.9001296
H	2.2073710	1.7771404	2.8951038
H	2.7428400	0.9542590	4.3862323
H	3.7713783	0.9274654	2.9363731

ax,eq-[VCl_3(l*i*Pr)$_2$]

Energy = -3246.262104 h

V	-0.6724559	-0.1317315	0.1539686
Cl	-1.4802152	-2.2705862	-0.1687683
Cl	-1.4809806	2.0094415	-0.1525283
Cl	-0.7946694	-0.1369967	2.4439831
C	-0.6893671	-0.1230724	-2.0685946
N	0.2685523	-0.1207418	-3.0286367
N	-1.8526857	-0.1197497	-2.7676355
C	-0.2822275	-0.1167955	-4.2955785
C	1.7077446	-0.1276820	-2.7943840
C	-1.6264147	-0.1159843	-4.1256259
C	-3.2021065	-0.1207388	-2.1929885
H	0.3164778	-0.1147807	-5.2014185
H	1.8023086	-0.1192891	-1.7027806
C	2.3525266	1.1333475	-3.3481159
C	2.3350769	-1.4066182	-3.3268144
H	-2.4292100	-0.1128720	-4.8567359
H	-3.0542537	-0.1243608	-1.1051688
C	-3.9429586	-1.3912832	-2.5771483
C	-3.9413657	1.1532349	-2.5687137
H	3.4158491	1.1676983	-3.0685548
H	2.2962203	1.1732850	-4.4473531
H	1.8564826	2.0291361	-2.9474559
H	2.2738547	-1.4653341	-4.4249654
H	3.3987765	-1.4500006	-3.0498887
H	1.8282231	-2.2881659	-2.9084952
H	-4.9181557	-1.4187041	-2.0699547
H	-4.1282103	-1.4423706	-3.6620919
H	-3.3670395	-2.2738088	-2.2669403
H	-3.3644604	2.0329150	-2.2523294
H	-4.1262240	1.2118976	-3.6533413
H	-4.9166713	1.1783623	-2.0616129
C	1.4657907	-0.1346757	0.4212319
N	2.2575632	0.9389859	0.6669870
N	2.2558996	-1.2087921	0.6702690
C	3.5070903	0.5437888	1.0873966
C	1.8253530	2.3406689	0.5916088
C	3.5060132	-0.8140562	1.0894730
C	1.8223068	-2.6104121	0.5998302
H	4.2918368	1.2483780	1.3433491
H	0.9332134	2.3280129	-0.0505404
C	2.8899440	3.2078034	-0.0597107
C	1.4087019	2.8390269	1.9661244
H	4.2896851	-1.5190379	1.3476192
H	0.9300068	-2.5990139	-0.0420746
C	1.4060099	-3.1042087	1.9761036
C	2.8859555	-3.4808023	-0.0487707
H	2.4749775	4.2091816	-0.2423897
H	3.7750538	3.3367002	0.5831645
H	3.2167816	2.7931167	-1.0242007
H	2.2681167	2.8658785	2.6555028
H	0.9985221	3.8556581	1.8827640
H	0.6314259	2.1864980	2.3889770
H	0.9956781	-4.1210578	1.8960112
H	2.2656728	-3.1292589	2.6652473
H	0.6291605	-2.4500955	2.3972494
H	3.2134899	-3.0695749	-1.0144656
H	3.7707524	-3.6088352	0.5947161
H	2.4697772	-4.4822282	-0.2284048

6) References

[1] a) F. Basuli, U. J. Kilgore, X. Hu, K. Meyer, M. Pink, J. C. Huffman, D. J. Mindiola, *Angew. Chem. Int. Ed.* 2004, **43**, 3156-3159; (Angew. Chem. 2004, **116**, 3218 –3221.); b) F. R. Neururer, S. Liu, D. Leitner, M. Baltrun, K. R. Fisher, H. Kopacka, K. Wurst, L. J. Daumann, D. Munz, S. Hohloch, *Inorg. Chem.* 2021, **60**, 15421-15434; c) C. Lorber, L. Vendier, *Dalton Trans.* 2009, **35**, 6972-6984; d) J. Telser, C. C. Wu, K. Y. Chen, H. F. Hsu, D. Smirnov, A. Ozarowski, J. Krzystek, *J. Inorg. Biochem.* 2009, **103**, 487-495; e) T. A. Bazhenova, L. V. Zorina, S. V. Simonov, V. S. Mironov, O. V. Maximova, L. Spillecke, C. Koo, R. Klingeler, Y. V. Manakin, A. N. Vasiliev, E. B. Yagubskii, *Dalton Trans.* 2020, **49**, 15287-15298.

[2] a) F. Furche, R. Ahlrichs, C. Hättig, W. Klopper, M. Sierka, F. T. Weigend, *Mol. Sci.* 2014, **4**, 91-100; b) R. Ahlrichs, M. Bär, M. Häser, H. Horn, C. Kölmel, *Chem. Phys. Lett.* 1989, **162**, 165-169.

[3] a) O. Treutler, R. Ahlrichs, *J. Chem. Phys.* 1995, **102**, 346-354; b) M. Häser, R. Ahlrichs, *J. Comp. Chem.* 1989, **10**, 104-111.

[4] a) S. Grimme, J. Antony, S. Ehrlich, H. Krieg, *J. Chem. Phys.* 2010, **132**, 154104; b) A. D. Becke, E. R. Johnson, *J. Chem. Phys.* 2005, **123**, 154101; c) E. R. Johnson, A. D. Becke, *J. Chem. Phys.* 2006, **124**, 174104; d) S. Grimme, S. Ehrlich, L. Goerigk, *J. Comp. Chem.* 2011, **32**, 1456-1465; e) E. R. Johnson, A. D. Becke, *J. Chem. Phys.* 2005, **123**, 024101.

[5] a) J. P. Perdew, K. Burke, M. Ernzerhof, *Phys. Rev. Lett.* 1996, **77**, 3865; b) J. P. Perdew, M. Ernzerhof, K. Burke, *J. Chem. Phys.* 1996, **105**, 9982-9985; c) C. Adamo, V. Barone, *J. Chem. Phys.* 1999, **110**, 6158-6170; d) M. Ernzerhof, G. E. Scuseria, *J. Chem. Phys.* 1999, **110**, 5029-5036; e) J. Tao, J. P. Perdew, V. N. Staroverov, G. E. Scuseria, *Phys. Rev. Lett.* 2003, **91**, 146401; f) J. P. Perdew, J. Tao, V. N. Staroverov, G. E. Scuseria, *J. Chem. Phys.* 2004, **120**, 6898-6911.

[6] a) A. Schäfer, H. Horn, R. Ahlrichs, *J. Chem. Phys.* 1992, **97**, 2571-2577; b) A. Schäfer, C. Huber, R. Ahlrichs, *J. Chem. Phys.* 1994, **100**, 5829-5835; c) K. Eichkorn, O. Treutler, H. Oehm, M. Häser, R. Ahlrichs, *Chem. Phys. Lett.* 1995, **242**, 652-660; d) F. Weigend, R. Ahlrichs, *Phys. Chem. Chem. Phys.* 2005, **7**, 3297-3305; e) F. Weigend, *Phys. Chem. Chem. Phys.* 2006, **8**, 1057-1065.

[7] P. Deglmann, *Chem. Phys. Lett* 2004, **384**, 103-107.